Stability of combustion waves in the Zeldovich-Liñán model

V.V. Gubernov[a,*], A.V. Kolobov[a], A.A. Polezhaev[a], H.S. Sidhu[b]

[a] *I.E. Tamm Theory Department, P.N. Lebedev Physical Institute of Russian Academy of Sciences, Moscow 119991, 53 Leninskii prosp., Russian Federation*
[b] *School of Physical, Environmental and Mathematical Sciences, University of New South Wales at the Australian Defence Force Academy, Canberra, ACT 2600, Australia*

Abstract

In this paper we investigate the stability of the premixed combustion waves in the Zeldovich-Liñán model in the adiabatic limit in two spatial dimensions. It is shown that either wave or cellular instabilities emerge for the Lewis number for fuel greater or smaller than one respectively. On the Lewis number for fuel vs activation energy parameter plane, the critical parameter curve for wave (cellular) instability is a monotonically decaying (increasing) function, which tends to one for large values of activation energies and grows infinitely (vanishes) as the activation energy is decreased to some critical value (zero). Decreasing the recombination parameter, which corresponds to the relation between the characteristic times of the branching and recombination reactions, makes the combustion waves more stable by increasing the region of parameter values for stable travelling wave solutions. Increasing the ambient temperature is demonstrated to have similar stabilizing effect on combustion waves. The effect of the varying the Lewis number for radicals is shown to be more complex and depends on the regime of recombination. It is demonstrated that as the critical parameter values for the onset of instability are crossed, either pulsating or cellular two-dimensional solutions emerge. The properties of these solutions are studied. A comparison of the results of this paper with known data from the literature for deflagration of

*Corresponding author. Address: P.N. Lebedev Physical Institute of Russian Academy of Sciences, Moscow 119991, 53 Leninskii prosp., Russian Federation, Tel.: +7(499)132-6978, Fax: + 7(499) 135 8533

Email addresses: gubernov@lpi.ru (V.V. Gubernov), kolobov@lpi.ru (A.V. Kolobov), apol@lpi.ru (A.A. Polezhaev), h.sidhu@adfa.edu.au (H.S. Sidhu)

hydrogen-oxygen mixtures is made.

Keywords: premixed flames, combustion instabilities, Zeldovich-Liñán model, chain-branching reaction

1. Introduction

The Zeldovich-Liñán model was introduced by Zeldovich in 1948 [1]. It was the first two-step chain branching reaction model of premixed flame propagation, which included not only the initial species and products, but also intermediate species, i.e. radicals. Such reaction kinetic schemes are of special interest since hydrocarbon-air and hydrogen-air flames normally produce a pool of radicals through the branching reaction steps. The radicals later recombine to produce heat and products. These flames are usually modelled with chain-branching reaction kinetics. The model was analyzed by Liñán [2] using the activation energy asymptotics (AEA). Therefore this model is usually referred to as the Zeldovich-Liñán model. It comprises a chain branching reaction $A + B \rightarrow 2B$, and a chain-breaking (or recombination) reaction $B + B + M \rightarrow 2P + M$, where A is the fuel, B is the intermediate radical, P is the product, and M is a third body of collision needed for recombination, which is not changed by the reaction. It is assumed that the first reaction has a large activation energy and negligible heat of the reaction whereas, the recombination reaction has zero activation energy and is exothermic. The condition of zero heat release of the first reaction was subsequently relaxed in [3].

In [2] it was shown that there are three flame regimes in the Zeldovich-Liñán model: fast, slow and intermediate recombination. In the fast recombination regime the production of radicals by the branching step is much slower than the consumption of radicals through the recombination step. This has the following consequences: chain-branching and chain-recombination take place in the same thin reaction zone, the concentration of radicals is asymptotically small, and therefore the steady state approximation can be applied to it. In the slow recombination regime, the concentration of radicals is of the order of unity and all radicals are produced in a thin reaction zone. The consumption of radicals proceeds in a long scale region greater or comparable to the convection-diffusion region. In the intermediate recombination regime, the rates of the branching and termination reactions are comparable. The concentration of radicals is of the order of the dimensionless burned temper-

ature. The branching reaction takes place in a thin zone, which is followed by a much thicker recombination region. Both reaction zones are embedded in even larger convection-diffusion zones.

Using the above arguments, various asymptotic expansions have been introduced in different flame zones. The resulting asymptotic differential equations are then solved either symbolically or numerically depending on the complexity of the system of equations appearing as a result of asymptotic analysis. The model considered in [2, 3] does not include heat loss and the response curves obtained in these papers are single-valued functions. In [4] the Zeldovich-Liñán model with heat loss to the surroundings was considered by using AEA. It was demonstrated that the flame speed as a function of other parameters of the problem is a C-shaped function which exhibits turning point-type extinction condition similar to that predicted by the one-step nonadiabatic model [5].

In a number of investigations [6, 7, 8, 9], the influence of stretch on premixed flame for the Zeldovich-Liñán model was studied. The authors considered several distinguished limits in order to examine the problem in terms of AEA either analytically or semi-analytically. As a result it was found that the flame response to stretching depended upon the particular flame regime i.e. slow, fast or intermediate recombination.

In [10] Zeldovich introduced a slightly modified model with the kinetic scheme: $A + B \to 3B$ and $B + B + M \to 2P + M$, to describe the hydrogen-oxygen flame. Here A is the concentration of the deficient component and B is the concentration of the H atoms which are considered as the only radical involved in the reaction. Approximate formulas for the deflagration speeds were obtained in the limits of strong and weak recombination. Recently [11, 12] these results were tested using numerical calculations with detailed mechanism of the reaction and it was demonstrated that the two-step reaction model gives a good approximation of the flame propagation velocity. As discussed in [11, 12] the rate of the global recombination reaction is governed by two elementary steps: one being linear while the other is quadratic with respect to the radical concentration. In [10], Zeldovich considered the square-law route of radical recombination. This reaction path can be important for the case of hydrogen-rich mixtures. The applicability of the Zeldovich-Liñán model for the description of the hydrogen-rich flames is further described below. The linear elementary reaction step, where the H-radicals recombine with the oxygen molecules, has a higher reaction rate and must be faster in conditions with excess O_2. This reaction path should be dominating in the

case of lean mixtures. The chain-branching models with first-order recombination reactions have become very popular in the last decade. Partly, this is due to the fact that despite the apparent success in the investigation of the speed of the combustion waves, the stability of flames in the Zeldovich-Liñán model has not been systematically investigated, whereas for the models with first-order reaction, like the model introduced in [13], both the properties and stability of the travelling combustion waves can be studied using AEA.

A simplified version of the Zeldovich-Liñán model with first-order recombination reaction was introduced in [13] and studied analytically by AEA. The speed of the combustion wave was determined as a function of the parameters of the problem and was shown to be C-shaped in the nonadiabatic case. For the adiabatic case, the expression derived in [13] suggests a unique flame speed. The stability analysis was also carried out and two types of instability are expected to occur depending on the parameter values. For the case of the reactant Lewis number less than one, the analysis in [13] predicted that the wave could lose stability due to the emergence of cellular instabilities. The oscillatory instability is found for Lewis number greater than one. Recently a similar model [14] was studied in the adiabatic limit for the case of finite activation energies and the onset of cellular instabilities for Lewis number for fuel smaller than one was confirmed.

In [15, 16] we investigated the properties of the model introduced in [13] in the one-dimensional adiabatic case and in the limit of equal diffusivities of the reactant, the radical and heat. In [17, 18] the latter assumption was dropped. We demonstrated that when the Lewis number for fuel is less than unity the flame speed is unique and is a monotonically decreasing function of the dimensionless activation energy. As the flame speed decreases to zero, the combustion wave is stable with respect to one-dimensional perturbations and exhibits extinction for finite values of activation energy. For fuel Lewis number greater than unity the flame speed is a double-valued function. The slow solution branch is shown to be unstable whereas the fast solution branch is either stable or exhibits the onset of pulsating instabilities via the Hopf bifurcation. In [19] the analysis is generalized to the nonadiabatic case in two-spatial dimensions. It is demonstrated that the flame speed as a function of parameters is a double-valued C-shaped function regardless of the values of Lewis numbers. The slow solution branch is always unstable to uniform perturbations. For Lewis number for fuel greater than one, the fast solution branch is either stable or loses stability due to the wave or uniform perturbations. In [19, 20] complex regimes of flame propagation such as pul-

sating, chaotic, and standing waves are studied. These solutions are shown to emerge as a result of the loss of stability of the combustion wave with respect to oscillatory instability. In [21] the spherical geometry is studied and flame initiation and propagation is investigated. In [22] the model was extended to take into account the hydrodynamic effect induced by thermal expansion. The governing reaction-diffusion equations constituting the core of the model in [13] were coupled to the quasi-isobaric Navier-Stokes equations of the gas dynamics. It was shown by means of AEA that the flame always has a band of perturbations with small wavelength which are unstable due to the hydrodynamic mode.

However the kinetics can change the properties of combustion waves significantly and the results obtained for the model introduced in [13] cannot be directly applied to the Zeldovich-Liñán model. For example, in [23] it was found that the flame speed is a unique and monotonically decreasing function of the activation energy and the combustion wave does not exhibit extinction as the activation energy is increased. The results were compared to known predictions of the AEA and were found to agree. This is in contrast to the properties of the combustion waves in the adiabatic model introduced in [13]. In [23] the first attempt to tackle the stability of combustion waves in the Zeldovich-Liñán model in the one-dimensional case was undertaken. It was demonstrated that combustion waves lose stability due to the presence of supercritical Hopf bifurcations. The neutral stability boundary was found in the space of parameters. It was demonstrated that critical Lewis number for fuel is a monotonically decreasing function of the activation energy, which tends to one as the activation energy is asymptotically increased, and to infinity as the activation energy is decreased to certain finite critical value. The situation resembles the properties of the one-step adiabatic model, rather than the two-step chain branching model with the first-order recombination [13], where the bifurcation of co-dimension two was observed [20, 19].

The aim of the work presented in the current paper is to extend the results of the previous investigation [23] of the stability of the combustion waves in the Zeldovich-Liñán model from one to two spatial dimensions. In contrast to [23] both regions of Lewis numbers for fuel greater and less than one are considered. This allows the study of the emergence of cellular instabilities. The other goal of the current investigation is to determine the regimes of flame propagation which emerge as the travelling combustion wave becomes unstable. The paper is organized as follows. In section 2 the governing equations

and boundary conditions for the model are introduced in both dimensional and dimensionless forms. The properties of the travelling combustion waves are discussed. The linear stability analysis of these solutions is carried out in section 3. In section 4 the pulsating and cellular solutions that emerge as the neutral stability boundary is crossed in the space of parameters are investigated. In section 5 the parameters of the model are fitted to the deflagration of hydrogen-oxygen-argon mixtures. Conclusions are presented in section 6.

2. Model equations and travelling waves

We consider a diffusional thermal adiabatic model in two spatial dimensions that includes two steps: autocatalytic chain branching $A + B \to 2B$ and recombination $B + B + M \to 2P + M$. Following the approach of [1], it is assumed that all the heat of the reaction is released during the recombination stage and the chain branching stage does not produce or consume any heat. According to [4], the dimensional equations governing this process can be written as

$$\begin{aligned}
\rho c_p \frac{\partial T}{\partial t} &= \lambda \Delta T + q_F W_A A_R \left(\frac{\rho Y_B}{W_B}\right)^2 \frac{\rho Y_M}{W_M}, \\
\rho \frac{\partial Y_A}{\partial t} &= \rho D_A \Delta Y_A - W_A A_B \left(\frac{\rho Y_A}{W_A}\right)\left(\frac{\rho Y_B}{W_B}\right) e^{-E/RT}, \\
\rho \frac{\partial Y_B}{\partial t} &= \rho D_B \Delta Y_B + \frac{\rho Y_B}{W_B}\left(A_B \frac{\rho Y_A}{W_A} e^{-E/RT} - 2A_R \frac{\rho Y_B}{W_B}\frac{\rho Y_M}{W_M}\right) W_B,
\end{aligned} \tag{1}$$

where $\Delta = \partial^2/\partial x^2 + \partial^2/\partial y^2$; T is the temperature; Y_A and Y_B represent the mass fraction of fuel and radicals respectively; ρ is the density; λ is the thermal conductivity; c_p is the specific heat; D_A and D_B represent the diffusivities of the fuel and radicals respectively, A_R and A_B are constants of recombination and chain branching reactions respectively; W_A, W_B, and W_M represent the molecular weights of fuel, radicals and a third body; q_F is the specific heat of the recombination reaction; E is the activation energy for the chain branching reaction; R is the universal gas constant. Eqs. (1) are considered subject to boundary conditions

$$\begin{aligned}
&T = T_a, \qquad Y_A = Y_A^\infty, \qquad Y_B = 0 \quad \text{for} \quad x \to +\infty, \\
&dT/dx = 0, \quad dY_A/dx = 0, \quad Y_B = 0 \quad \text{for} \quad x \to -\infty,
\end{aligned} \tag{2}$$

which correspond to a wave travelling in the positive x-axis direction. A more detailed discussion of the boundary conditions is given below, while describing the numerical integration scheme. Upstream, on the right boundary, T is equal to the ambient temperature, T_a; fuel has not been consumed yet and Y_A is equal to its maximal initial value in the cold unreacted mixture, Y_A^∞; no radicals have been produced i.e. $Y_B = 0$. Downstream, on the left boundary, we require that there is no reaction happening, so the solution reaches a stationary point of Eq. (1). Therefore the zero flux conditions for T, Y_A, and zero condition for Y_B are imposed.

Introducing the nondimensional time, $t' = (\rho A_B / e^\beta \beta M^*)t$, coordinate $\mathbf{r}' = (\rho^2 A_B c_p / \lambda M^* \beta e^\beta)^{1/2}\mathbf{r}$, variables

$$u = \frac{T}{T^*\beta}, \quad v = \frac{Y_A}{Y_A^\infty}, \quad w = \frac{Y_B W_A}{Y_A^\infty W_B}, \tag{3}$$

and dimensionless parameters

$$\beta = \frac{2Ec_p}{Rq_F Y_A^\infty}, \quad L_{A,B} = \frac{\lambda}{D_{A,B}\rho c_p}, \quad r = \frac{2A_R Y_M \rho e^\beta}{A_B W_M}, \tag{4}$$

where $M^* = W_A/Y_A^\infty$ and $T^* = q_F Y_A^\infty / 2c_p$ is the reference mass and temperature respectively, β is the dimensionless activation energy, L_A and L_B are the Lewis numbers for fuel and radicals respectively, we write Eqs. (1) and (2) omitting primes as

$$\begin{aligned} u_t &= \Delta u + r w^2, \\ v_t &= L_A^{-1}\Delta v - \beta v w \exp\left(\beta - 1/u\right), \\ w_t &= L_B^{-1}\Delta w + \beta v w \exp\left(\beta - 1/u\right) - r\beta w^2, \end{aligned} \tag{5}$$

and

$$\begin{aligned} &u = u_a, \qquad v = 1, \qquad w = 0 \quad \text{for} \quad x \to +\infty, \\ &du/dx = 0, \quad dv/dx = 0, \quad w = 0 \quad \text{for} \quad x \to -\infty. \end{aligned} \tag{6}$$

It should be noted that time and space non-dimensionalization in Eq. (4) is different from the one used in [23]. This results in the multiplier e^β in the branching reaction rate in Eq. (5) and a different definition of the recombination parameter, r, which corresponds to parameter R in [23].

The properties of the travelling combustion waves are numerically studied in detail in [23]. Here we briefly outline the main results. The solution to the problem (5)-(6) is sought in the form of a travelling wave $u(\mathbf{r},t) = u(\xi)$, $v(\mathbf{r},t) = v(\xi)$, and $w(\mathbf{r},t) = w(\xi)$, where a coordinate in the moving frame, $\xi = x - ct$, is introduced and c is the speed of the travelling wave. It is found that the flame speed is unique, the combustion wave does not exhibit extinction as the activation energy is increased in contrast to the model with the first order recombination reaction [16]. The flame speed is a monotonically decreasing function of the activation energy. The structure of the travelling combustion wave is found to depend on the recombination parameter, r, which has a physical meaning of the ratio of the characteristic times of the branching and recombination reactions. For small values of r, the slow recombination regime of flame propagation is observed. In this case the leading edge of the flame is governed by heat and species diffusion, the reaction zone consists of a thin branching zone embedded in a much wider recombination region. In the branching zone almost all the fuel is converted to radicals and the radical concentration reaches values of the order of $O(1)$. In the recombination region the radicals are transformed into products and heat is released. The recombination reaction spreads to the product zone, where the recombination, rather than the transport effects are dominating. As a result the temperature and species concentrations approach the asymptotic values in sub-exponential manner. This distinguishes the Zeldovich-Liñán model from both the one-step and other two-step reaction models. In the case of large r, the recombination reaction is faster than the branching reaction and the fast recombination regime of flame propagation is observed. In the upstream region the transport effects are dominating. This preheat zone is followed by the reaction region, where the recombination reaction follows the branching reaction and a steady-state approximation applies to the radical species. As a result, the radical concentration is small. The two-step reaction model can be reduced to the one-step reaction model with second-order reaction and by doubling the activation energy of that for the branching reaction in the two-step model. The reduced model allows the AEA analysis which results in the following asymptotic formula for the flame speed (see [23] and references therein)

$$c = \frac{L_A}{\beta\sqrt{2r}}, \tag{7}$$

which differs from the corresponding expression in [23] due to the different

nondimensionalization used here. It is clear from Eq. (7) that such a choice of nondimensional parameters eliminates the exponential dependence of the flame speed on β and is more convenient for numerical investigation of the properties of the travelling combustion waves for large values of activation energies. The properties of the travelling wave solution described above are illustrated in Fig. 1, where the dependencies of the flame speed (panel a) and the maximum value of the radical concentration, w_{max}, (panel b) are plotted versus β for $L_A = L_B = 1$ and different values of the recombination parameter $r = 0.02$ and $r = 50.0$. In Fig. 1 (a) the solid lines represent the numerical results and the dotted lines correspond to the predictions of the asymptotic formula (7). It is seen that the correspondence is good for the fast recombination regime and large activation energies. In the slow recombination regime the discrepancy between the one-step and two-step models is substantial reaching two orders of magnitude. In Fig. 1 (b) the dependence of $w_{max}(\beta)$ is shown. It is seen that for $r = 0.02$ the maximal value of radical concentration becomes comparable to the fuel concentration for moderate values of β and decrease as β becomes larger. On the other hand for $r = 50$ the radical concentration is almost three orders of magnitude smaller which qualitatively agree with the prediction of the AEA for fast recombination regime.

The dependence of the combustion wave speed on other parameters has been studied in [23]. In particular, the variation of L_A affects the combustion wave substantially, so that the combustion wave travels faster for larger values of L_A. In contrast, the variation of L_B has almost no effect on the flame speed. The next section is devoted to a stability analysis of the combustion waves.

3. Linear stability

In order to investigate the stability of the combustion waves with respect to the pulsating perturbations we linearize the governing Eqs. (5) near the travelling wave solution. We seek solution of the form $u(\mathbf{r}, t) = U(\xi) + \epsilon\phi(\xi)\exp(\lambda t + iky)$, $v(\mathbf{r}, t) = V(\xi) + \epsilon\psi(\xi)\exp(\lambda t + iky)$, and $w(\mathbf{r}, t) = W(\xi) + \epsilon\chi(\xi)\exp(\lambda t + iky)$, where $[U(\xi), V(\xi), W(\xi)]$ represent the travelling combustion wave. Here terms proportional to the small parameter ϵ are the linear perturbation terms, λ is a spectral parameter governing the time evolution of the perturbation and k is the wave number which is transverse to the wave propagation direction. The main difference of our current approach from the earlier investigation [23] is that two-dimensional perturbations are

allowed here. Substituting this expansion into Eq. (5), leaving terms proportional to the first order of ϵ only, and introducing the vector function with components $\mathbf{v}(\xi) = [\phi,\ \psi,\ \chi,\ \phi_\xi,\ \psi_\xi,\ \chi_\xi]^T$ we obtain

$$\mathbf{v}_\xi = \hat{A}(\xi, \lambda, k)\mathbf{v}, \tag{8}$$

where

$$\hat{A} = \begin{bmatrix} 0 & \hat{I} \\ \hat{H} + k^2\hat{I} + \lambda\hat{Q} & -c\hat{Q} \end{bmatrix}, \quad \hat{Q} = \begin{bmatrix} 1 & 0 & 0 \\ 0 & L_A & 0 \\ 0 & 0 & L_B \end{bmatrix}, \tag{9}$$

$$\hat{H} = \begin{bmatrix} 0 & 0 & -2rW \\ \dfrac{\beta L_A V W}{U^2 e^{1/U}} & \dfrac{\beta L_A W}{e^{1/U}} & \dfrac{\beta L_A V}{e^{1/U}} \\ \dfrac{-\beta L_B V W}{U^2 e^{1/U}} & \dfrac{-\beta L_B W}{e^{1/U}} & L_B\left(\dfrac{-\beta V}{e^{1/U}} + 2\beta r W\right) \end{bmatrix}, \tag{10}$$

Here $\hat{I}$ is 3×3 identity matrix, $U(\xi)$, $V(\xi)$, $W(\xi)$ are functions of the ξ-coordinate and represent the travelling combustion wave. We will call a set, Σ, of all λ values for which there exists a solution to Eq. (8) bounded for both $\xi \to \pm\infty$ a spectrum of linear perturbations. In the general case, Σ is a set on the complex plane and it consists of the essential and the discrete spectrum. If there exists at least one $\lambda \in \Sigma$ such that $\mathrm{Re}\lambda > 0$, then the travelling wave solution is linearly unstable, otherwise, if for all $\lambda \in \Sigma$ the real parts are not positive, then the travelling wave solution is linearly stable. Therefore in order to investigate the linear stability of the travelling wave solutions to Eq. (5), the spectrum Σ of the problem (8) has to be found for all k values. It can be shown (see [24] for details) that the essential spectrum consists of parabolic curves in the complex plane with $\mathrm{Re}\lambda \leq 0$. This implies that it is the discrete spectrum of the problem (8) that is responsible for the emergence of instabilities.

The linear stability problem is solved by finding the location of the discrete spectrum on the complex plane using the Evans function method [24] implemented with the use of a compound matrix approach (see [18] for more details). From the mathematical point of view, (8) is an eigenvalue problem for a system of Ordinary Differential Equations with asymptotically constant

coefficients exhibiting the so-called exponential dichotomies: for each λ outside the essential spectrum, the solution space of (8) can be presented as a direct sum of the subspaces of the solutions bounded, E_s^+, and unbounded, E_u^+, as $\xi \to \infty$. The same is true in the opposite limit $\xi \to -\infty$ and $C^n = E_s^- \bigoplus E_u^-$. Then, λ is an eigenvalue (or a point of the discrete spectrum) if the subspace of solutions, E_s^- (bounded for $\xi \to -\infty$) intersects nontrivially with the subspace of solutions, E_s^+ (bounded for $\xi \to \infty$). In our case, for all λ located in the complex plane to the right from the essential spectrum, both subspaces are three dimensional and therefore can be represented by 3-vectors, $\mathbf{V}^{\pm}$, respectively. The Evans function is then defined as $E(\lambda) \sim \mathbf{V}^+ \wedge \mathbf{V}^-$, where $\mathbf{V}^{\pm}$ are evaluated at a certain value of ξ. The 3-vectors, $\mathbf{V}^{\pm}(\xi)$ are evaluated numerically via the compound matrix method (see [18] and references therein). According to [24] the problem of locating points of the discrete spectrum is equivalent to the problem of finding zeros of the Evans function, $E(\lambda)$, on the complex plane. In contrast to the one-dimensional stability analysis, where the discrete spectrum is a set of points for fixed parameter values, the present analysis in two dimensions results in the solutions to Eq. (8) having $\lambda(k)$ dependencies (the dispersion relations). In general, $\lambda(k)$ is a complex function of real variable. Analogous to [19], depending on the behaviour of $\lambda(k)$ instabilities of two types are expected to occur: wave or cellular instabilities.

The results of the linear stability analysis are presented in Fig. 2. For the case of fuel Lewis number greater than one, the combustion wave loses stability with respect to perturbations of the wave type. In this case, as the neutral stability boundary is crossed in the parameter space the maximum value of the $\mathrm{Re}\lambda(k)$ dependence, which is reached at certain $k = k_{max} > 0$, becomes positive and corresponding value of $\mathrm{Im}\lambda(k_{max}) \neq 0$. This situation is illustrated in the inset of Fig. 2 (in the top-right corner), where $\mathrm{Re}\lambda(k)$ and $\mathrm{Im}\lambda(k)$ are schematically shown. The marginal values for the wave instability are plotted with solid line for various values of r ranging from 0.02 to 50 and $L_B = 1$, $u_a = 0$. The impact of the latter parameters is described below. In each case stable combustion waves exist for the parameter region below the solid curves. The critical parameter values for the Hopf bifurcation, which is encountered in the one-dimensional formulation and studied in [23], are also given in the figure for the same parameter values and are shown with the dotted lines. It is seen that the wave instabilities of the multidimensional nature dominate the one-dimensional pulsating instabilities and are encountered in the parameter space before the critical values for the Hopf bifurcation has

been reached. The neutral stability boundary $L_A(\beta)$ is a monotonically decaying function of hyperbolic type: for large values of activation energy the critical value of L_A tends to 1; on the other hand as β approaches the critical value, β_{tr}, the Lewis number for fuel exhibits unbounded growth. The location of the neutral stability boundary is qualitatively similar to the case of the one-step adiabatic model. For the slow recombination regime, $r < 1$, the variation of the recombination parameter substantially affects the stability of combustion waves: as r is decreased the neutral stability boundary shifts to larger values of the activation energy. For the case of fast recombination, $r > 1$, the neutral stability boundary tends to limiting curve. For instance, the increase of r from 10 to 50 results in only a slight modification of the critical parameters $L_A(\beta)$ from curve 4 to 5 in Fig. 2.

The properties of the wave instability such as the spatial structure in the transverse direction and time frequency of oscillations are determined by the parameters k_{max} and $\omega_{max} = \mathrm{Im}\lambda(k_{max})$ of the dominating instability i.e. the mode of the linear stability problem (8) for which maximum of $Re(\lambda) > 0$ is reached at $k = k_{max}$. These parameters are important since they characterize the properties of the complex solutions emerging as a result of the primary bifurcation as the travelling combustion wave loses stability. In Fig. 3 the dependence of the wave number (a) and frequency of oscillations (b) on the activation energy are plotted for the dominating instability. Parameters k_{max} and ω_{max} are sampled for each value of β at the neutral stability boundary i.e. L_A is adjusted in each case so that L_A and β correspond to the marginal values for the onset of wave instability. Other parameter values are fixed as indicated in the figure caption. Both $k_{max}(\beta)$ and $\omega_{max}(\beta)$ are monotonically decaying functions. As the recombination parameter is decreased, higher values of the wave number and frequency of the dominating instability are observed. Since the marginal dominating instability mode can be a precursor of the bifurcating solution in the soft excitation regime, we can expect the structures with larger transverse scales and slower temporal dynamics to emerge as the recombination parameter is increased.

For the case of $L_A < 1$, the analysis shows that the combustion wave loses stability with respect to cellular perturbations. This type of instability does not have a one-dimensional analogue and is exhibited in systems with at least two-dimensional geometry. The characteristic dispersion relation for cellular instability is schematically shown in the inset to Fig. 4 in the right-bottom corner. The real part of $\lambda(k)$ is only presented on the graph since the imaginary part is equal to zero. For stable travelling waves, the

dependence of $\mathrm{Re}\lambda(k)$ is a monotonically decreasing function anchored at the origin, $\lambda(0) = 0$. As the neutral stability boundary is approached, the inclination of the $\mathrm{Re}\lambda(k)$ graph at $k = 0$ tends to zero and diminishes as the critical parameters are reached. Crossing the neutral stability boundary from the stable to unstable region of parameters results in the change of the sign of the inclination (or derivative) of $\mathrm{Re}\lambda(k)$ at $k = 0$ from negative to positive. As a consequence there appears an extremum in the $\mathrm{Re}\lambda(k)$ function at a certain value of $k = k^*$ as illustrated in the inset to Fig. 4. It should be noted that the dispersion relation is always anchored at the origin in this case i.e. $\lambda(0) = 0$. In Fig. 4 the critical parameter values for the onset of cellular instabilities are plotted on the L_A versus β plane for $L_B = 1$, $u_a = 0$ and several values of r ranging from 0.02 to 50. The corresponding regions of stable combustion waves are located above the marginal curves for cellular instability. The neutral stability boundary, $L_A(\beta)$, is a monotonically increasing function. The behaviour of the critical parameter curve $L_A(\beta)$ looks qualitatively similar to the case of the one-step adiabatic model: as β tends to zero, L_A diminishes and as β becomes large, L_A tends to one. The region of stable combustion waves shrinks and the marginal curve elevates as the recombination parameter is increased from 0.02 to 1. For $r > 1$ a tendency to certain limiting behaviour is observed: changing r from 10 to 50 only slightly affects the critical parameters, so that the corresponding neutral stability curves lie almost on top of each other.

It should be noted that the stability results governing the onset of pulsating and cellular instabilities described above are consistent with those obtained for a single-step adiabatic models. In [25, 26, 27, 28] the AEA analysis of the flame stability in diffusional-thermal approximation was carried out. These predictions were later verified numerically [29]. The neutral stability boundaries for the onset of cellular and pulsating flames qualitatively agree with those shown in Figs. 2 and 4.

The influence of varying L_B on the stability of combustion waves is also investigated for both slow and fast recombination regimes (for brevity, the results are not shown here). The increase of L_B has a rather complex effect upon the critical parameters for wave instability ($L_A > 1$) in the case of slow recombination. For intermediate values of the activation energies the critical parameter values shift towards larger values of β with the increase of L_B i.e. for heavier radicals the flame is less stable. On the other hand for large β the opposite tendency is observed: increasing L_B moves the neutral stability back towards smaller β. For the case of cellular instability ($L_A < 1$)

the situation is less ambiguous: decreasing L_B makes the combustion wave more stable. The same result, although less pronounced, is observed for the case of fast recombination. As noticed earlier, when r becomes large the stability characteristics seem to tend to some limiting behaviour. As a result the increase of L_B only slightly decreases the region of stability of the combustion waves for both $L_A < 1$ and $L_A > 1$.

The ambient temperature, u_a, is an important experimental parameter. In the studies above it was fixed to zero. Next we investigate the impact of this parameter on the stability of the travelling wave solutions. In Fig. 5 the neutral stability boundary is plotted on the L_A versus β plane for $r = 0.1$, $L_B = 1$, and two values of the ambient temperature $u_a = 0$ and $u_a = 0.01$. The case of wave instabilities, $L_A > 1$, is presented in panel (a). Here the solid line corresponds to the neutral stability boundary and the dotted line represents the Hopf bifurcation for the one-dimensional case. It is seen that the increase of the ambient temperature shifts the stability curve to the region of larger β values, thus making the combustion waves more stable. The onset of cellular instabilities is demonstrated in panel (b) of Fig. 5. It follows from graphs for $u_a = 0$ and 0.01 that raising the temperature of the surroundings has stabilizing influence on the flame. This effect is more evident for larger values of the activation energy and becomes less apparent for intermediate and small values of β. Fig. 6 is similar to Fig. 5 with the only difference being that a fast recombination is considered i.e. $r = 10$. In panel (a) the case of $L_A > 1$ is presented. It is seen that in contrast to varying L_B, changing u_a still has a significant effect on the stability boundaries. The same situation is observed in panel (b), where the cellular instability curves are presented for $u_a = 0$ and 0.01. Increasing the ambient temperature has a stabilizing effect by shifting the neutral stability boundary to lower values of L_A.

4. Standing and cellular waves

We investigate the properties of the emerging combustion wave solutions when the parameters cross the neutral stability boundary for the travelling wave solutions. The governing Eqs. (5) are solved in a sufficiently large rectangular coordinate region with the boundary conditions (6) imposed at the edges of the space grid along the y-axis and zero flux conditions for u, v, and w for the edges along the x-axis. The length of the region along the x-direction is chosen to be sufficiently large so that the boundary conditions

(6) are satisfied with reasonable accuracy. The length of the region in the y-direction is chosen to accommodate one period of the transverse perturbation structure. For our numerical algorithm we use the method of splitting with respect to physical processes. Initially we solve the set of ordinary differential equations which describe the temperature and the variations of species concentration due to the branching and recombination reactions by using a fourth-order Runge-Kutta algorithm. Next, the equations of heat and mass transfer for fuel and radicals are solved by the method of alternating directions with the Crank-Nicholson scheme. The initial conditions are taken in the form of the travelling wave solution (or autowave) of Eq. (5).

As shown in the previous section, depending on the Lewis number for fuel there can emerge two types of instabilities: wave instabilities for $L_A > 1$ or cellular instabilities for $L_A < 1$. We consider the solutions bifurcating from the travelling waves separately in these parameter regions.

4.1. Wave instabilities and standing waves

As the critical parameter values for the wave instability ($L_A > 1$) are crossed in the parameter space a pulsating travelling solution emerges due to a primary bifurcation. This type of solution is illustrated in Fig. 7, where contours of the radical concentration profile $w(x, y)$ are plotted for three successive moments of time $t_1 = 80$, $t_2 = 145$, and $t_3 = 190$. In Fig. 7 only a part of the integration domain $x \in [360, 410]$ is presented for illustrative purposes, whereas the whole range of integration used in the numerical scheme was $x \in [0, 2000]$. The level curves correspond to $w = 0.02$, 0.06, 0.1, 0.14, 0.18, 0.22 and 0.26. For the parameter values shown in the figure caption the critical activation energy for the onset of wave instability is $\beta = 6.668...$, the time period of pulsations is $T \approx 108$, and the space period of the solution in the transverse direction is about 100, which agrees well with the prediction of the linear stability analysis. In Fig. 7 the offset propagation coordinate, $x - \overline{c}t$, is shown, where $\overline{c}$ is the average flame propagation velocity, i.e. the time average of the flame position over a period does not change. The sampling time, t_i, is done so as to cover one period of oscillation and to show the evolution of the characteristic radical concentration profile along a single period. As seen in Fig. 7, once the neutral stability boundary is crossed in parameter space the planar travelling wave solution exhibits both time pulsations and flame front segmentation in the transverse direction. This results in the formation of soliton-type radical "hotspots".

In Fig. 7(a) there is a single spot located at $y = 50$. As long as there is a sufficient amount of fuel in this region the concentration of the radicals grows while the maximum remains at the same location. Increased radical concentration results in faster recombination, local heating, and the formation of local temperature maxima . The temperature increase accelerates the branching reaction and leads to a local depletion of the fuel concentration. As a result the w_{max} growth changes to a decay of the radical concentration maxima. While w_{max} is high the recombination reaction is still active and the temperature is growing. This is illustrated in Fig. 8, where the dynamics of $u_{max}(t)$ and $w_{max}(t)$ are shown in panel (a) and the dependence of the location of w_{max} in the coordinate plane (x_{max}, y_{max}) is plotted with diamonds connected with the solid line in panel (b) for the same parameter values as in Fig. 7. It should be noted that two peaks of radical concentration in Fig. 8(a) correspond to a single period of pulsations. Also in panel (b) of the same figure only a half-interval of the integration domain along the y-axis is shown since the rest of the figure can be obtained by symmetry. This phase in the system dynamics corresponds to the profile (a) in Fig. 7 and is also marked in Fig. 8 as t_1. The increase in local temperature is accompanied by a flame speed acceleration, which results in the advancement of the location of the radical spot towards higher values of the coordinate x. At a certain stage the heat release stagnates as w_{max} becomes small and the decay in u_{max} is observed. The radical hotspot cannot propagate along the x-axis since the fuel is substantially depleted in the local region near $y = 50$. On the other hand, on both sides of this peak of radical concentration along the y-axis there is an excess amount of unburned fuel. The epicentre of the reaction splits into two peaks which depart from the location at $y = 50$ towards the outer edges of the integration domain i.e. to $y = 0$ and $y = 100$ lines. This corresponds to the radical concentration profile in Fig. 7(b) as well as to the part of the trajectories marked as t_2 in Fig. 8(b). As the radical spots move along these paths away from the line $y = 50$, the maximum local radical concentration and temperature decay, the relative spot velocities become smaller and they retard towards smaller values of the x-coordinate in Fig. 8(b). By the time of the arrival of spots to the outer boundaries of the integration domain, $y = 0$ and $y = 100$, the radical concentration passes through a local minimum and a different trend is observed: approaching fuel-rich regions near the boundaries intensifies the branching reaction and w_{max} begins to regain its high values. At this stage the spots remain at the same positions along y-axis and start to advance forward to larger x values. The growth of the radical concentration

increases the heat release and the local temperature. The temperature rise triggers the branching reaction, so that the fuel becomes locally depleted. The maximum of $w_{max}(t)$ is reached, followed by its subsequent decay. This phase corresponds to Fig. 7(c) and points marked t_3 in Fig. 8. The dynamics is then repeated periodically forming a standing wave-like pattern. In our numerical calculations, tens of periods of such pulsations have been observed without any drift in the parameters of such oscillations.

It should be noted that the onset of pulsating solutions was also investigated for single-step models. In [26, 27, 28] the AEA nonlinear stability analysis was carried out and it was shown that the planar pulsating waves emerge as a result of the supercritical Hopf bifurcation. These results were also verified numerically [30, 31]. In [32, 33] a model of gasless solid fuel combustion of a cylindrical sample was considered. It was assumed that combustion occurs only on the surface of the cylinder which resulted in two-dimensional formulation of the problem. Numerical study showed that various types of propagating solid flames exist as parameters of the problem are varied, including uniformly propagating planar flames, pulsating planar flames, and flames exhibiting more complex spatiotemporal dynamics such as different modes of hot spots propagation. These regimes are qualitatively similar to standing waves reported here.

The properties of the bifurcation giving rise to standing wave solutions is also studied. As the activation energy is increased from the critical value β_c, which is 6.668... in Fig. 7-8, pulsations in $w_{max}(t)$ appear. These oscillations are small for $\beta - \beta_c \ll 1$ and are well described by the frequency $\mathrm{Im}\lambda$ obtained from the linear stability analysis. The amplitude of oscillations grow according to a root law as β is increased. The temperature oscillations are small and the amplitude of pulsations do not exceed the level of several percent from the adiabatic combustion temperature even for the relatively large $\beta - \beta_c$ values. As for the fuel concentration profile, there are no notable peaks or troughs appearing as a result of the onset of standing waves. However there emerges a phase shift along the y-direction as the critical bifurcation parameter value is crossed. This is observed as a change in the pulsating front curvature in contrast to the previously planar travelling wave prior to bifurcation. As the bifurcation parameter is increased the characteristics of the standing wave, frequency of pulsations and wave length in the y-direction, exhibit mild deviations from the values prescribed by the linear stability analysis, $\mathrm{Im}\lambda$ and k^{-1} of the dominating instability. The average flame speed, $\overline{c}$, of the standing wave is smaller than the velocity of the un-

stable travelling wave solution for the same parameter values. This agrees with the results reported in [20].

4.2. Cellular instabilities and waves

For the case, $L_A < 1$, cellular instabilities emerge as the neutral stability boundary is crossed in parameter space. In contrast to the wave instability, in this case the dispersion relation calculated at the critical parameter values does not provide the characteristic time and transverse length scales of the cellular perturbation. For parameter values slightly beyond the stability boundary, there appears an unstable mode with very weak coefficient of exponential growth and large wave numbers. As we further modify the parameters, for example by increasing β, and move away from the bifurcation conditions the wave number in the y-axis direction and the growth rate, $\mathrm{Re}\lambda$, of the dominating instability becomes larger. As a result the emergence of the cellular instabilities becomes tractable with direct numerical integration of the governing Eq. (5).

Initially, the instabilities cause minor deviations of the flame front which resulted in the front being no longer planar, but corrugated. This fragmentation of the flame front is also accompanied by the variations of the peak value of the radical concentration along the y-axis. Variations of the temperature and fuel profiles are less pronounced. After integration of the governing equations over times of the order of several $(\mathrm{Re}\lambda)^{-1}$, which is 10^5 in the order of magnitude, the solution relaxes to a stationary cellular wave, which travels with constant speed along the x-axis without changing its shape in the coordinate frame travelling with the wave. A typical cellular wave is demonstrated in Fig. 9, where a contour plot of the radical concentration, $w(x,\ y)$, is shown for $L_A = 0.81$, $L_B = 1$, $\beta = 9.5$, and $r = 0.1$. Here x is the co-moving coordinate travelling with the flame. The level curves correspond to $w = 0.0125$, 0.025,..., 0.075. As in the previous contour plots, only part of the integration domain $x \in [400, 470]$ is presented in Fig. 9. The whole range of integration was $x \in [0, 800]$. The length of the domain in the y-direction is chosen to accommodate a single cellular structure. It should be noted that for the parameter values in Fig. 9 the travelling wave losses stability at $\beta_c = 5.55...$ Although the bifurcation parameter, β, is substantially altered from this critical value in Fig. 9 the variation in the peak values of the radical concentration along the y-axis, $\Delta w_y = \max_y[\max_x w] - \min_y[\max_x w]$, reaches only several percent of its maximum value. This is clearly seen from the location of the level curves in Fig. 9. The nature of bifurcation is also

different from the case $L_A > 1$, since Δw_y grows linearly with the increase of the bifurcation parameter, β. For the temperature and fuel concentration profiles the cellular structure manifests only in the shift of the phase of the front along the y-axis (or nonzero curvature of the flame front), whereas no appreciable peaks are observed in the u and v distributions. Interestingly, the speed of the cellular wave and the travelling wave solution (which is unstable) are equal up to the numerical accuracy for determining the front velocity. This, in addition to large times required for onset of cellular solutions from the travelling wave solutions, makes this type of numerical study of cellular structures very difficult.

5. Hydrogen-oxygen combustion

Although to date there is a good understanding of the hydrogen oxidation chemistry which includes eight chemical species [34, 35], there is still a lack of short reduced mechanisms for modelling the problems with multi time and length scales such as studying the flame stability and time dependent regimes of flame propagation. One of the first models of the H_2 - O_2 mixture combustion was proposed in [10]. This model included the branching $A + B \rightarrow 3B$ and the recombination $B + B + M \rightarrow P + M$ steps, where A is the deficient component concentration, for example, O_2, B is the H atom concentration which is considered as the only radical involved in the reaction. In [36] the steady-state approximation for O, OH and HO_2 was adopted and a similar model was derived and investigated for rich hydrogen-oxygen flames. In this case the rate of the first global reaction is governed by the elementary step $H + O_2 \rightarrow OH + H$ and the rate of the second global reaction is governed by elementary reaction $H + H + M \rightarrow H_2 + M$. In [37] the two-step reaction mechanism was further developed. It was shown to be capable of producing reasonably accurate predictions for the flame structure and speed as compared to the data obtained from both the detailed chemistry calculations and experiments. The two-step mechanism was used in [38] to study the asymptotic structure of premixed hydrogen-air flames. Recently in [11, 12], the model was tested using numerical calculations with detailed mechanism of the reaction and it was demonstrated that the two-step reaction model gives a good approximation of the flame propagation velocity. As discussed in [11, 12], the rate of H recombination is governed by two elementary reactions $H + H + M \rightarrow H_2 + M$ and $H + O_2 + M \rightarrow HO_2 + M$. The H-radical recombination with O_2 has a higher rate and

must be faster in the presence of appreciable oxygen concentration. The square-law termination reaction however, could play a substantial role in the case of hydrogen rich mixtures and/or slow recombination regimes when the concentration of H atoms becomes significant and O_2 is rapidly depleted in the course of fast branching. In [39], the mechanism was further modified to include an initiation reaction $H_2 + O_2 \rightarrow HO_2 + H$ and to relax the equilibrium assumption for hydroperoxyl radical. The resulting model was found to be suitable for analysing deflagration, autoignition and diffusion hydrogen-air flames. It should also be noted that in the limit of lean hydrogen air flames the steady state approximation can be applied to the H radicals as well and the mechanism can be reduced to just a single-step reaction scheme as was demonstrated in [40].

In [12] a detailed kinetic calculation for the stationary propagating flame in a 26/13/61 mixture of $H_2/O_2/Ar$ was carried out at pressure below 1 atm. Here we estimate the main parameters of such flames based on the Zeldovich approach and compare these predictions with the detailed kinetic analysis data from [12]. The governing equations in this case are similar to Eq. (1), where in the third equation the branching rate should be doubled as in equation (1) of [11]. This is due to a different stoichiometry of the global branching reaction. Next, we introduce the nondimensional variables Eq. (3) and (4), where the reference temperature and mass are now equal to $T^* = q_F Y_H / c_p$ and $M^* = W_A / 2Y_A^\infty$ respectively. Here A refers to O_2 and B to H, $Y_H = 2Y_A^\infty W_B / W_A$ is the characteristic scale for the radical concentration, so that $w = Y_B / Y_H$. The dimensionless activation energy is now $\beta = E c_p / q_F R Y_H$. Substituting these definitions into Eq. (1) we obtain Eq. (5). The thermodynamic and kinetic data for the elements of the gas mixture and the rates of the elementary steps involved in the overall two-step kinetic mechanism are obtained from the NIST database [41, 42]. We consider the case of the ambient temperature $T_a = 370$K and pressure $p = 1$ atm as in [12]. This gives the following values for the dimensionless parameters: $\beta \approx 3.9$, $r \approx 0.002$, $L_A \approx 2$, and $L_B \approx 0.3$. These values are within the range of parameters considered in the current article and correspond to the stable travelling combustion wave with slow recombination regime and low recombination parameter value, which is also the case for [12]. We undertake numerical calculations with the given set of parameters and recast the results back to the dimensional form which yields the flame speed, $c \approx 4$ m/s and the burned temperature $T_b \approx 2600$K. This is very close to the flame speed, $c = 3.8$ m/s obtained in [12] using the Zeldovich asymptotic

analysis approach. However, both approaches give higher values of the flame velocity in comparison to the numerical calculations using the detailed kinetic scheme, which is 3.37 m/s according to [12]. The characteristic distributions of molar concentrations of species and temperature are plotted in Fig. 10 for the case of $p = 1$ atm. Although there are no data for direct comparison, there appears to be good qualitative correspondence to the results reported in [12, 43]. For instance, in [12] the maximum concentration of H is estimated as ≈ 0.09 using the Zeldovich asymptotic analysis and ≈ 0.08 by direct numerical calculation based on the detailed kinetics. In our calculations this value is 0.107.

6. Conclusions

In this article the stability of premixed combustion waves in the two-dimensional Zeldovich-Liñán model is considered in the adiabatic limit. For given parameter values the combustion wave has a unique speed. The structure of the travelling combustion wave is found to depend on the recombination parameter, r, showing the relation between the characteristic times of the branching and recombination reactions. For $r < 1$, the slow recombination regime of flame propagation is observed. For $r > 1$ the recombination reaction is faster than the branching reaction and the fast recombination regime is encountered. For fast recombination the asymptotic analysis gives a good prediction of the flame velocity.

The stability of the combustion waves in the Zeldovich-Liñán model was investigated by the Evans function method and by direct integration of the governing partial-differential equations. The results from both methods are found to agree with a high degree of accuracy. It was determined that the combustion wave loses stability due to either wave or cellular instabilities depending upon the Lewis number for fuel. The neutral stability boundary is found on the L_A versus β plane. For the case of $L_A > 1$, the combustion wave loses stability with respect to wave perturbations. The neutral stability boundary $L_A(\beta)$ is a monotonically decaying function, which tends to one for large values of activation energy and grows infinitely as β is decreased to some critical value. For the case of $L_A < 1$, the combustion wave loses stability with respect to cellular perturbations. The neutral stability boundary, $L_A(\beta)$, is a monotonically increasing function. As β tends to zero L_A diminishes and as β becomes large L_A tends to one. In both cases, the location of the neutral stability boundary is qualitatively similar to the results for the

one-step adiabatic model. An important experimental parameter, which is also present in the one-step models, is the ambient temperature. It is demonstrated that the initial preheating of the fresh mixture has a stabilizing effect on the combustion waves. The marginal boundary for the onset of wave instability shifts to larger values of β and the critical parameter values for cellular instability move to smaller L_A values. This results in the increase of the region of the stable travelling combustion waves in the parameter space and qualitatively agrees with the prediction of the one-step model.

Parameters L_B and r are specific to the Zeldovich-Liñán model and cannot be reproduced in the single reaction step analysis. The variation of the recombination parameter also has a strong effect on the stability of the combustion wave. For the slow recombination regime $r < 1$, the decrease of r shifts the neutral boundary to larger values of the activation energies for $L_A > 1$ and towards smaller values of β for the case $L_A < 1$. Thus reducing the recombination parameter stabilizes the combustion waves. As r is increased above unity, the region of stable travelling wave solutions becomes smaller. A tendency of the neutral stability boundary to certain limiting behaviour is observed i.e. increasing the recombination parameter by almost an order of magnitude only slightly alters the critical parameter values for both wave and cellular instabilities. The effect of varying L_B on the stability of combustion waves was also studied. For the fast recombination regime, an increase in L_B shrinks the region of stable combustion, i.e. for heavier radicals the flame is less stable. For the slow recombination regime, the same effect is observed for cellular instabilities, whereas for wave perturbations the behaviour is more complex and depends on β.

We would like to point out that our current study of the combustion waves in the Zeldovich-Liñán model, which possesses a second-order recombination reaction, has properties that are more common to the adiabatic one-step models. This is in contrast to the first-order recombination reaction studied in [13, 17, 18, 19, 20]. In the latter model, the existence of the combustion wave extinction and the presence of the Bogdanov-Takens bifurcation point are demonstrated even for the adiabatic case. Similar behaviour can be expected for the nonadiabatic Zeldovich-Liñán model [4] and the clarification of this issue is the subject of our future investigation. In other words, the kinetics of the recombination reaction, specifically the order of the reaction, has an effect on the properties and stability of the combustion waves.

It is shown that as the critical parameter values for the wave instabilities are crossed in the parameter space, pulsating two-dimensional solutions

emerge. For parameter values close to the neutral stability boundary the time period of oscillations and the transverse space period of the emerging solutions agree with the dominating wave instability characteristics obtained from the linear stability analysis. The primary bifurcation causing the emergence of the pulsating solutions is found to be of supercritical nature. In terms of the radical concentration, the travelling pulsating solutions have the structure of soliton-type radical spots which propagate along certain trajectories. In this paper we have considered the zero-flux conditions in the transverse direction and the length of the domain was chosen so as to accommodate a single period of the pulsating solution in the y-direction. Obviously, if different boundary conditions are imposed, solutions with more complex dynamics can emerge. The propagation of the standing wave solutions is accompanied by oscillations of the peaks of the concentration of radicals. The amplitude of such oscillations is found to follow the square-law dependence on the "beyond-critical" parameter (the difference between the current and marginal parameter values). The amplitude of oscillations for the radical concentration can reach the order of tens of percent from the maximum radical concentration. Although the temperature pulsations are an order of magnitude smaller than the oscillations of the radical concentration it still should be possible to observe these pulsations experimentally since the luminosity is proportional to the fourth power of temperature.

As the critical parameters for the onset of cellular instability are crossed in parameter space, a two-dimensional cellular wave bifurcates from the one-dimensional planar travelling wave solution. The cellular wave travels with constant speed without changing its shape in the co-moving coordinate frame. The flame speed for the cellular solution branch is found to coincide with the velocity of the planar travelling wave solution up to the numerical accuracy of our calculations, which was of the order of one percent for the determination of the front velocity. The radical concentration profile appears as a bell-shaped function of the longitudinal coordinate, whereas the peaks of the radical distribution are shifted in phase along the transverse coordinate i.e. a front corrugation occurs so that the radical profile looks as a curved front. The maximum values of the radical concentration in the longitudinal direction also vary as we change the transverse coordinate. These variations are relatively small and are of the order of several percent from the maximum value of the concentration of the radical. In contrast to the case of standing waves, the amplitude of such variations is found to be linearly dependent on the "beyond-critical" parameter. The temperature and fuel concentration

profiles differ from the travelling wave profiles in the curved structure of the fronts. There are no appreciable peaks of temperature in comparison to the travelling wave profiles. These properties of flame speed and structure of the cellular waves could obstruct their experimental observation, unless the parameters are substantially shifted away from the neutral stability boundary.

As follows from the preliminary comparison of the results with the data known from the literature, the Zeldovich-Liñán model has the potential to estimate the flame speed and feasibly reproduces the flame structure for the deflagration of hydrogen-oxygen mixture. Further investigation is required to apply this approach to different stoichiometries and to different physical conditions to validate the results with respect to experimental data for hydrogen-oxygen flames. Of special interest is undertaking such comparisons for the prediction of the limits of stability and emergence of pulsating and cellular flames with complex dynamics.

7. Acknowledgements

V.V. Gubernov, A.V. Kolobov and A.A. Polezhaev would like to acknowledge the financial support from the Russian Foundation for Basic Research grant 11-01-00392 and the Dynasty Foundation. H.S. Sidhu would like to acknowledge the support of the Australian Research Council Grant DP0878146.

References

[1] Y. B. Zeldovich, Zhurnal Fizicheskoi Khimii 22 (1948) 27–48.

[2] A. Liñán, A Theoretical Analysis of Premixed Flame Propagation with an Isothermal Chain Reaction, Technical Report 1, Instituto Nacional de Tecnica Aeroespacial Madrid (Spain), 1971.

[3] G. Joulin, A. Liñán, G. Ludford, N. Peters, C. Schmidtlaine, SIAM Journal on Applied Mathematics 45 (1985) 420–434.

[4] B. H. Chao, C. K. Law, International Journal of Heat and Mass Transfer 37 (1994) 673 – 680.

[5] G. Joulin, P. Clavin, Combustion and Flame 35 (1979) 139 – 153.

[6] K. Seshadri, N. Peters, Combustion Science and Technology 33 (1983) 35–63.

[7] D. W. Mikolaitis, Combustion Science and Technology 49 (1986) 277–288.

[8] R. Y. Tam, Combustion Science and Technology 60 (1988) 125–142.

[9] R. Y. Tam, Combustion Science and Technology 62 (1988) 297–309.

[10] Y. B. Zeldovich, Kinetika i kataliz 2 (1961) 305–318.

[11] D. Fernández-Galisteo, G. del Alamo, A. Sánchez, A. Liñán, in: Proc. of the Third European Combustion Meeting 2007, 6-19, pp. 1–5.

[12] O. Korobeinichev, T. Bolshova, Combustion, Explosion, and Shock Waves 45 (2009) 507–510. 10.1007/s10573-009-0061-1.

[13] J. W. Dold, Combustion Theory and Modelling 11 (2007) 909–948.

[14] G. J. Sharpe, SIAM Journal on Applied Mathematics 70 (2009) 866–884.

[15] V. V. Gubernov, H. S. Sidhu, G. N. Mercer, Journal of Mathematical Chemistry 39 (2006) 1–14.

[16] V. V. Gubernov, H. S. Sidhu, G. N. Mercer, Combustion Theory and Modelling 12 (2008) 407–431.

[17] V. V. Gubernov, H. S. Sidhu, G. N. Mercer, A. V. Kolobov, A. A. Polezhaev, Journal of Mathematical Chemistry 44 (2008) 816–830.

[18] V. V. Gubernov, A. V. Kolobov, A. A. Polezhaev, H. S. Sidhu, G. N. Mercer, International Journal of Bifurcation and Chaos 19 (2009) 873–887.

[19] V. V. Gubernov, A. V. Kolobov, A. A. Polezhaev, H. S. Sidhu, G. N. Mercer, Combustion Theory and Modelling 15 (2011) 385–407.

[20] V. Gubernov, A. Kolobov, A. Polezhaev, H. Sidhu, G. Mercer, Proceedings of the Royal Society A - Mathematical Physical and Engineering Sciences 466 (2010) 2747–2769.

[21] H. Zhang, Z. Chen, Combustion and Flame 158 (2011) 1520–1531.

[22] G. J. Sharpe, Combustion Theory and Modelling 12 (2008) 717–738.

[23] V. Gubernov, A. Kolobov, A. Polezhaev, H. Sidhu, Journal of Mathematical Chemistry (2011) 1–17. 10.1007/s10910-010-9797-9.

[24] B. Sandstede, in: B. Fiedler (Ed.), Handbook of Dynamical Systems II, Elsevier, North-Holland, 2002, pp. 983–1055.

[25] G. I. Sivashinsky, Combustion Science and Technology 15 (1977) 137–145.

[26] B. J. Matkowsky, G. I. Sivashinsky, SIAM Journal on Applied Mathematics 35 (1978) 465–478.

[27] B. J. Matkowsky, D. O. Olagunju, SIAM Journal on Applied Mathematics 39 (1980) 290–300.

[28] S. B. Margolis, B. J. Matkowsky, Combustion Science and Technology 34 (1983) 45–77.

[29] D. G. Lasseigne, T. L. Jackson, L. Jameson, Combustion Theory and Modelling 3 (1999) 591–611.

[30] K. G. Shkadinskii, B. I. Khaikin, A. G. Merzhanov, Combustion, Explosion, and Shock Waves 7 (1971) 15–22.

[31] R. Weber, G. Mercer, H. Sidhu, B. Gray, Proceedings of the Royal Society A - Mathematical Physical and Engineering Sciences 453 (1997) 1105–1118.

[32] A. Bayliss, B. Matkowsky, A. Aldushin, Physica D-Nonlinear Phenomena 166 (2002) 104–130.

[33] A. Bayliss, B. J. Matkowsky, V. A. Volpert, in: A. A. Golovin, A. A. Nepomnyashchy (Eds.), Advances in Sensing with Security Applications, volume 218 of *NATO Science Series*, Springer Netherlands, 2006, pp. 247–282.

[34] P. Saxena, F. A. Williams, Combustion and Flame 145 (2006) 316–323.

[35] M. O. Conaire, H. J. Curran, J. M. Simmie, W. J. Pitz, C. K. Westbrook, International Journal of Chemical Kinetics 36 (2004) 603–622.

[36] G. Dixon-Lewis, Royal Society of London Proceedings Series A 298 (1967) 495–513.

[37] F. Mauss, N. Peters, B. Rogg, F. A. Williams, in: N. Peters & B. Rogg (Ed.), Lecture Notes in Physics, Berlin Springer Verlag, 1993, volume 15 of *Lecture Notes in Physics, Berlin Springer Verlag*, pp. 29–43.

[38] K. Seshadri, N. Peters, F. A. Williams, Combustion and Flame 96 (1994) 407 – 427.

[39] P. Boivin, C. Jiménez, A. L. Sánchez, F. A. Williams, Proceedings of the Combustion Institute 33 (2011) 517 – 523.

[40] D. Fernández-Galisteo, A. L. Sánchez, A. Liñán, F. A. Williams, Combustion and Flame 156 (2009) 985 – 996.

[41] E. W. Lemmon, M. O. McLinden, D. G. Friend, in: P. Linstrom, W. Mallard (Eds.), NIST Chemistry WebBook, NIST Standard Reference Database Number 69, National Institute of Standards and Technology, Gaithersburg MD, 20899, http://webbook.nist.gov (retrieved August 15, 2011).

[42] J. A. Manion, R. E. Huie, R. D. Levin, D. R. Burgess Jr., V. L. Orkin, W. Tsang, W. S. McGivern, J. W. Hudgens, V. D. Knyazev, D. B. Atkinson, E. Chai, A. M. Tereza, C.-Y. Lin, T. C. Allison, W. G. Mallard, F. Westley, J. T. Herron, R. F. Hampson, D. H. Frizzell, in: NIST Standard Reference Database 17, Version 7.0 (Web Version), Release 1.4.3, Data version 2008.12, National Institute of Standards and Technology, Gaithersburg, Maryland, 20899-8320. Web address: http://kinetics.nist.gov/ (retrieved August 15, 2011).

[43] Y. B. Zeldovich, G. I. Barenblatt, V. B. Librovich, G. M. Makhviladze, The mathematical theory of combustion and explosions, Consultants Bureau, New York, 1985.

8. List of captions

Fig. 1 Dependencies of (a) the speed, c, of combustion wave and (b) the maximum value of the concentration of radicals, w_{max}, on the activation

energy, β, for two values of recombination parameter $r = 0.02$ and $r = 50$ and $L_A = L_B = 1$. Graphs are plotted in logarithmic scale.

Fig. 2 Stability diagram on L_A vs. β plane for $L_B = 1$, $u_a = 0$ and various values of $r = 0.02$, 0.1, 1, 10, and 50 shown with curves 1, 2, 3, 4, and 5, respectively. The solid and the dashed lines represent the critical parameter values for the emergence of wave instability and the one-dimensional Hopf bifurcation, respectively. The parameter region corresponding to stable solutions is located below the critical curves in each case. A sketch of a typical dispersion relation for the case of the wave instability is shown in the inset in the top-right corner.

Fig. 3 The dependence of k_{max} (a) and w_{max} (b) on β for $L_B = 1$, $u_a = 0$, $r = 10$ and $r = 0.1$.

Fig. 4 Stability diagram on the L_A vs. β plane for $L_B = 1$, $u_a = 0$ and various values of $r = 0.02$, 0.1, 1, 10, and 50. A sketch of a typical dispersion relation for the case of the cellular instability is shown in the inset in the bottom-right corner.

Fig. 5 Stability diagram in the L_A vs. β plane for $r = 0.1$, $L_B = 1$ and various values of $u_a = 0.0$ and 0.01 in case $L_A > 1$ (a) and $L_A < 1$ (b).

Fig. 6 Stability diagram on the L_A vs. β plane for $r = 10$, $L_B = 1$ and two values of $u_a = 0.0$ and 0.01 for the cases $L_A > 1$ (a) and $L_A < 1$ (b).

Fig. 7 Contour plots of the radical concentration profiles, $w(x,\ y)$, sampled at three successive moments of time $t_1 = 80$ in panel (a), $t_2 = 145$ in panel (b), and $t_3 = 190$ in panel (c) for $L_A = 10$, $L_B = 1$, $\beta = 7.5$, and $r = 0.1$.

Fig. 8 Panel (a) shows the values of the maximum radical concentration (diamonds connected with solid lines) and temperature (crosses connected with the dashed lines). Panel (b) shows the dependence of the location y versus x on the maximum of the radical concentration. The parameters are chosen as in Fig. 7. The moments of time at which the profiles are sampled in Fig. 7 are marked as dashed lines in (a) and are denoted by bold squares in (b).

Fig. 9 Contour plots of the radical concentration profiles, $w(x,\ y)$, for $L_A = 0.81$, $L_B = 1$, $\beta = 9.5$, $r = 0.1$.

Fig. 10 Concentration of H and O_2 (left axis) and temperature (right axis) profiles for combustion wave in 26/13/61 $H_2/O_2/Ar$ mixture at $p = 1$ atm.

Figure 1

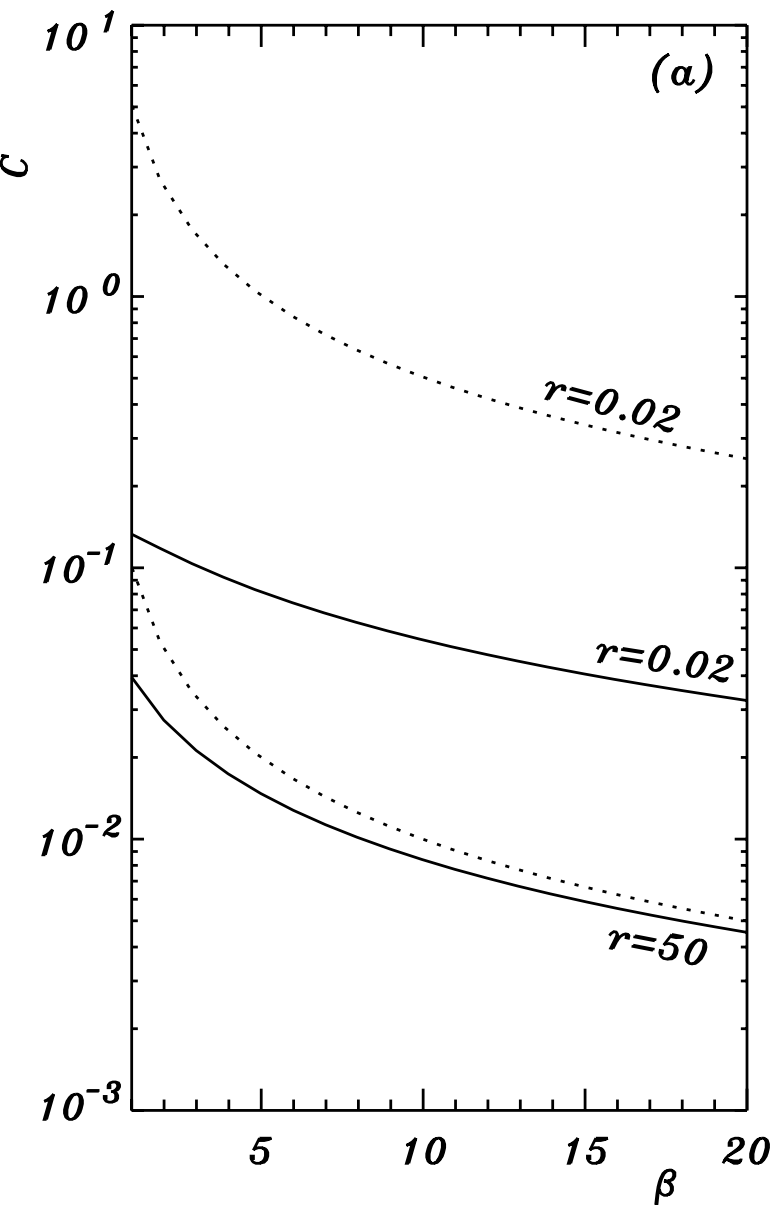

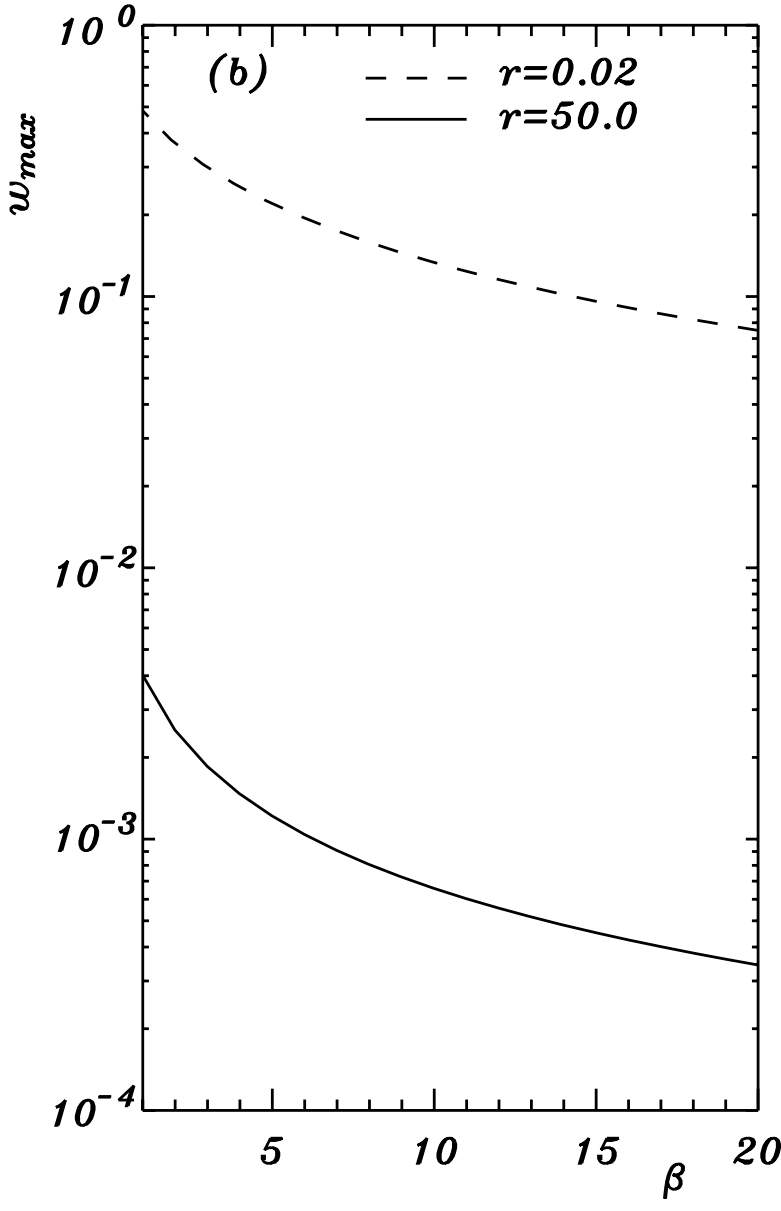

Figure 2

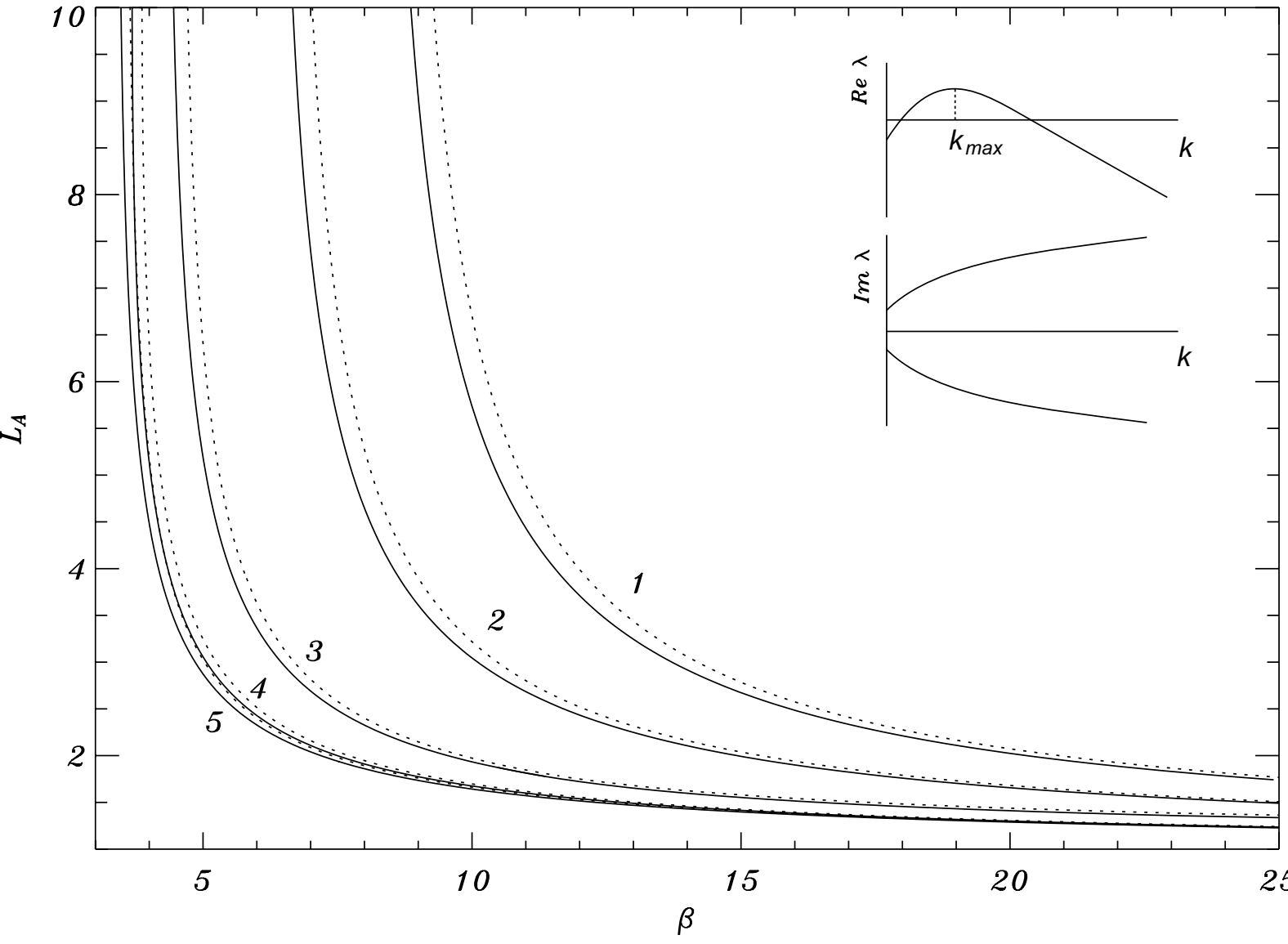

Figure 3

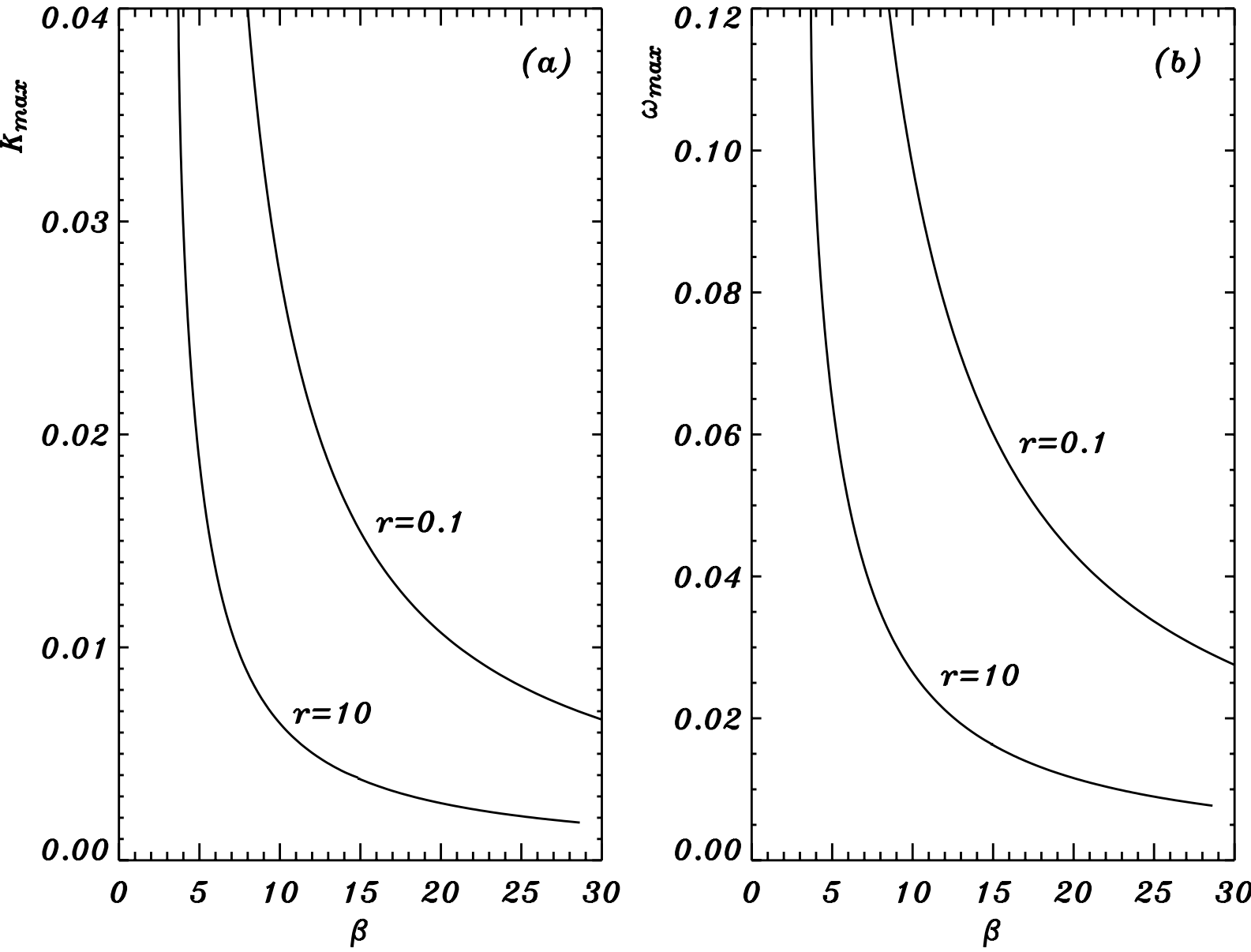
(a)
K_{max}
0.04
0.03
0.02
0.01
0.00
r=0.1
r=10
0
5
10
15
20
25
30
β
(b)
ω_{max}
0.12
0.10
0.08
0.06
0.04
0.02
0.00
r=0.1
r=10
0
5
10
15
20
25
30
β

Figure 4

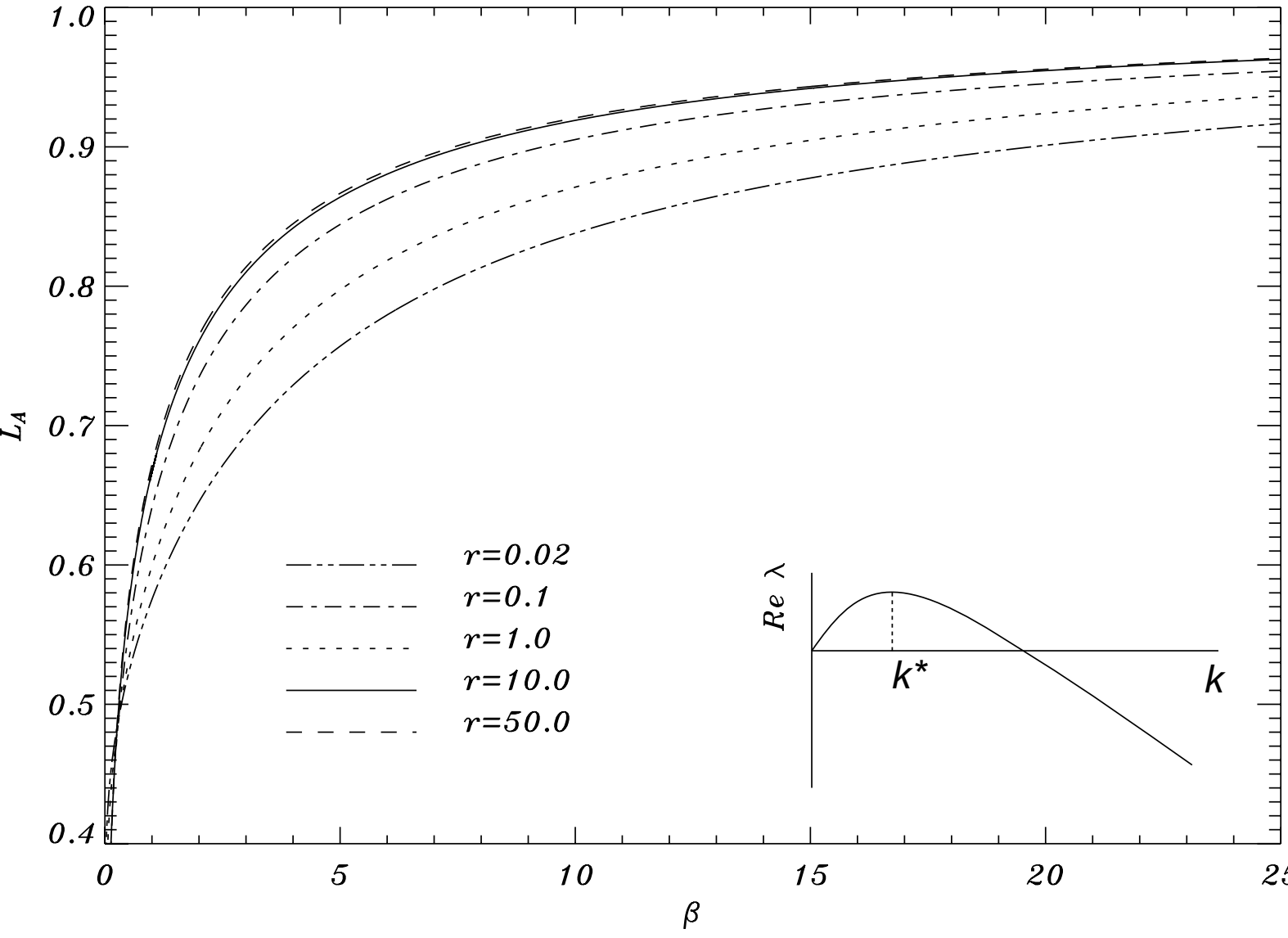
1.0
0.9
0.8
0.7
0.6
0.5
0.4
L_A
0
5
10
15
20
25
β
r=0.02
r=0.1
r=1.0
r=10.0
r=50.0
Re λ
k*
k

Figure 5

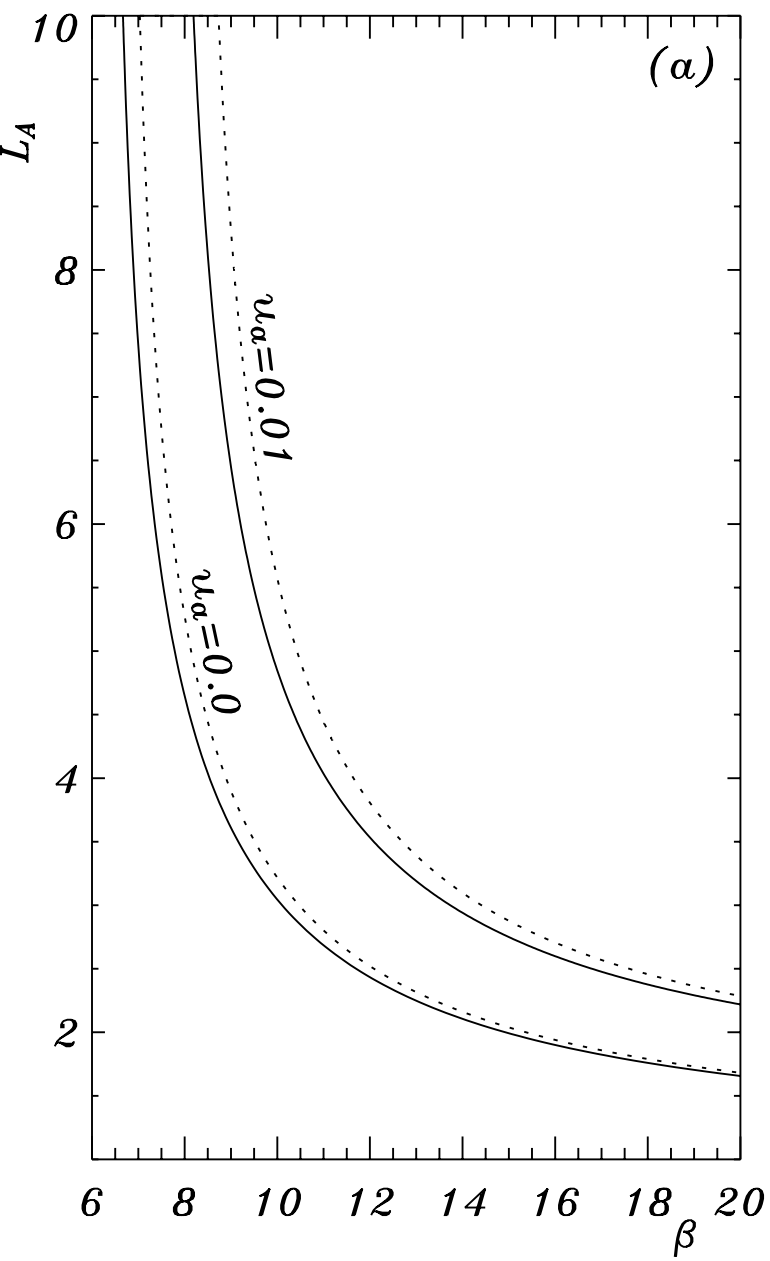
(a)
L_A
10
8
6
4
2
u_α=0.01
u_α=0.0
6
8
10
12
14
16
18
20
β

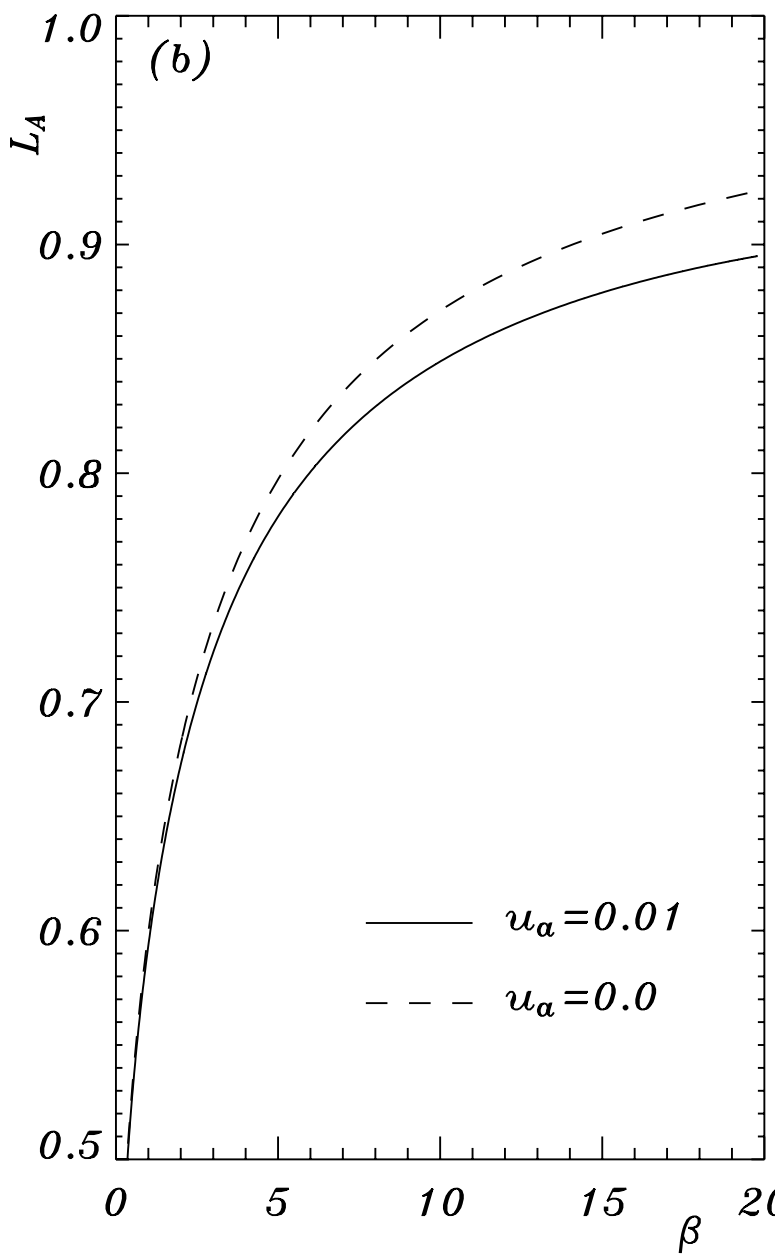
(b)
L_A
1.0
0.9
0.8
0.7
0.6
0.5
u_α=0.01
u_α=0.0
0
5
10
15
20
β

Figure 6

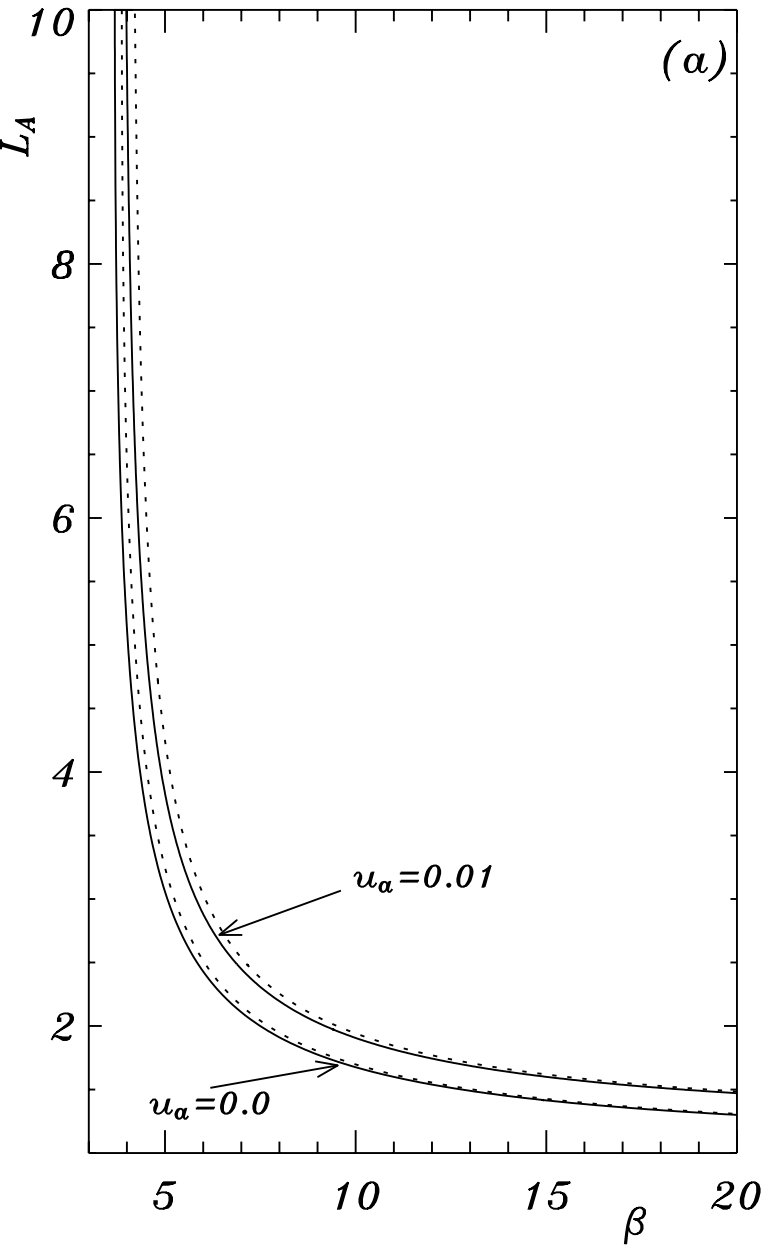
(a)
L_A
10
8
6
4
2
5
10
15
20
β
u_α=0.01
u_α=0.0

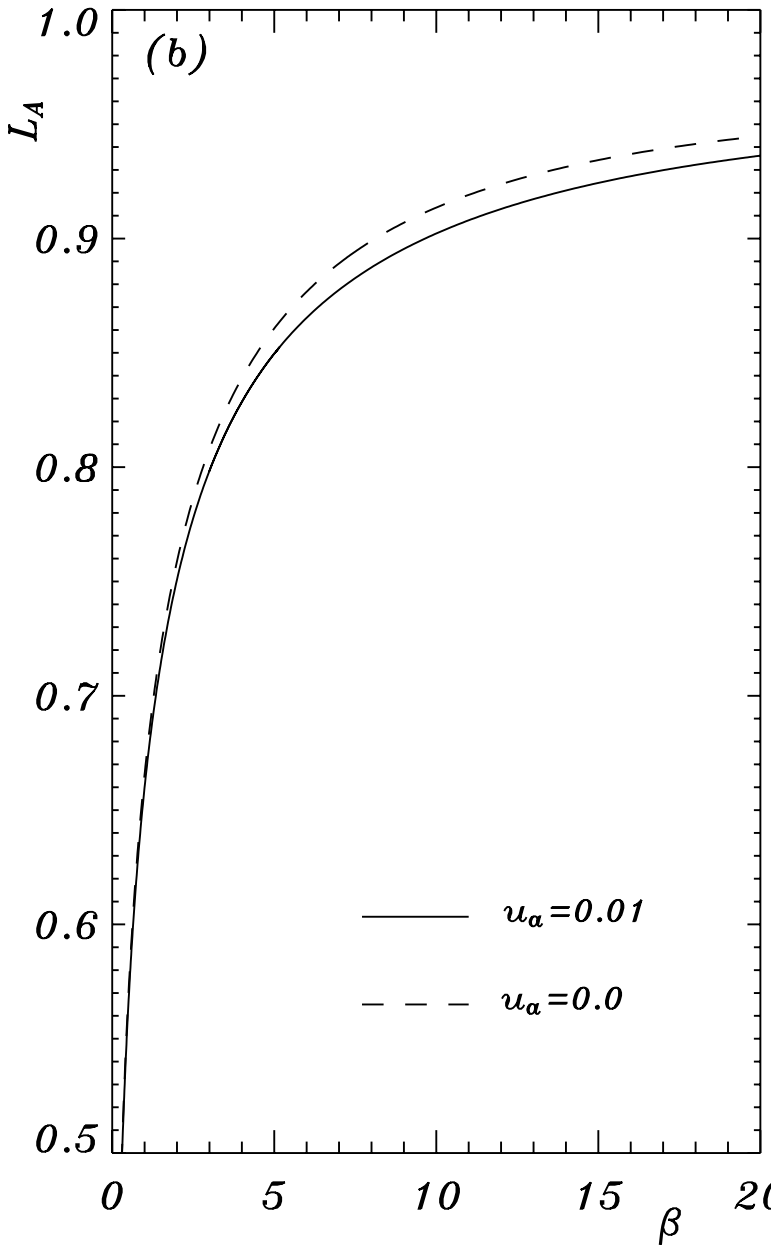
(b)
L_A
1.0
0.9
0.8
0.7
0.6
0.5
0
5
10
15
20
β
u_α=0.01
u_α=0.0

Figure 7

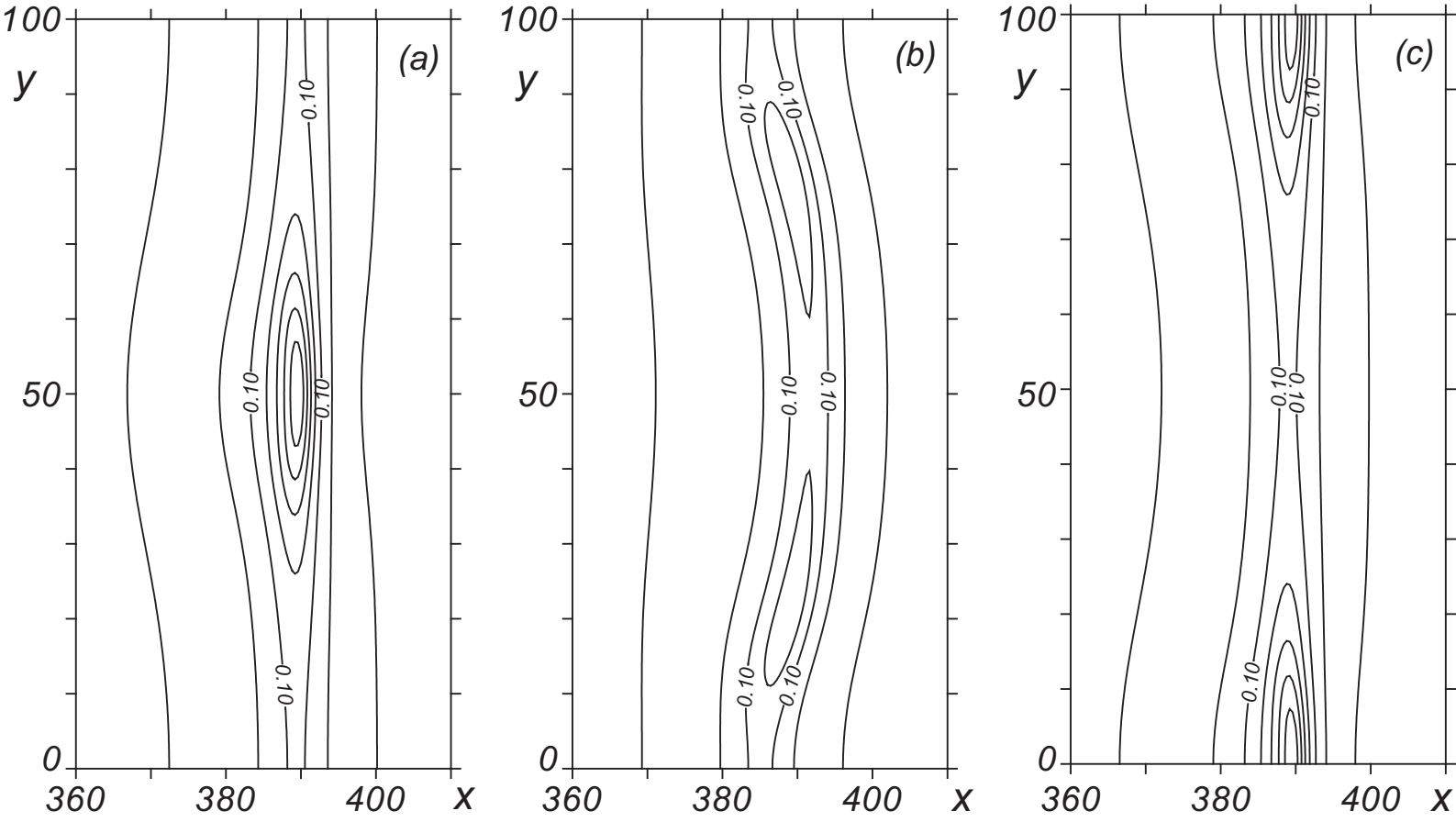

Figure 8

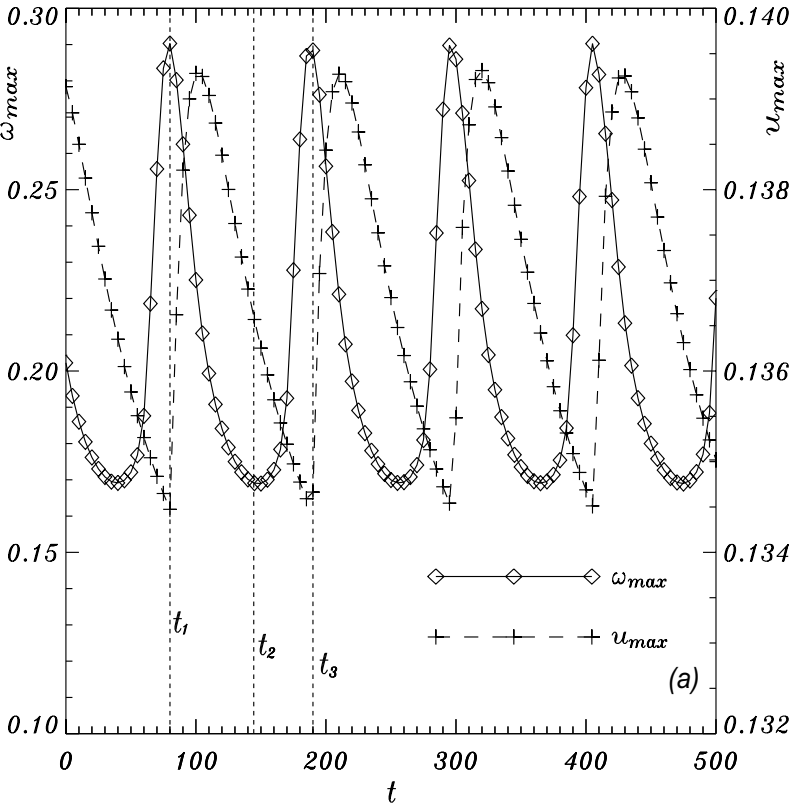
0.30
0.25
0.20
0.15
0.10
ω_{max}
0.140
0.138
0.136
0.134
0.132
u_{max}
0
100
200
300
400
500
t
t_1
t_2
t_3
ω_{max}
u_{max}
(a)

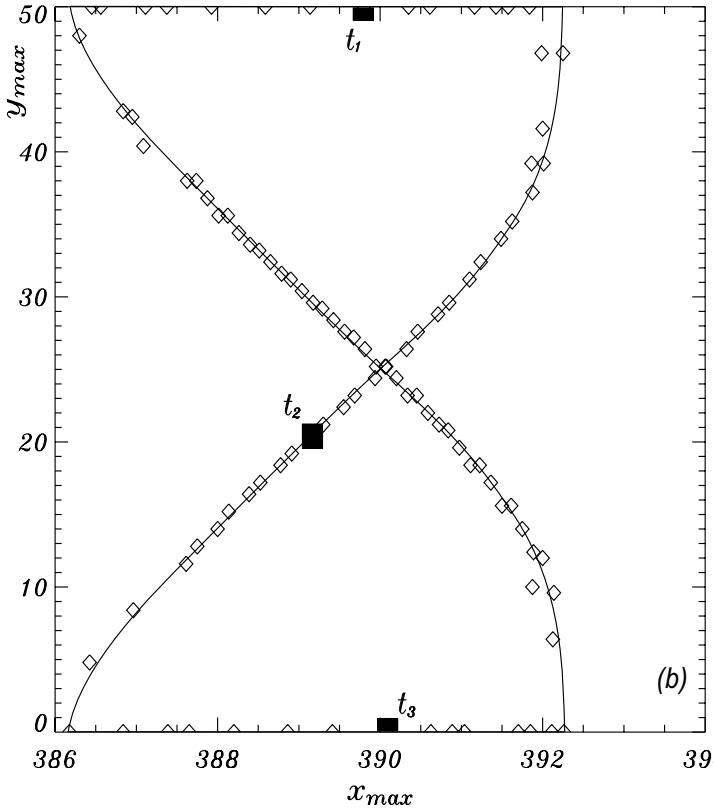
50
40
30
20
10
0
y_{max}
386
388
390
392
394
x_{max}
t_1
t_2
t_3
(b)

Figure 9

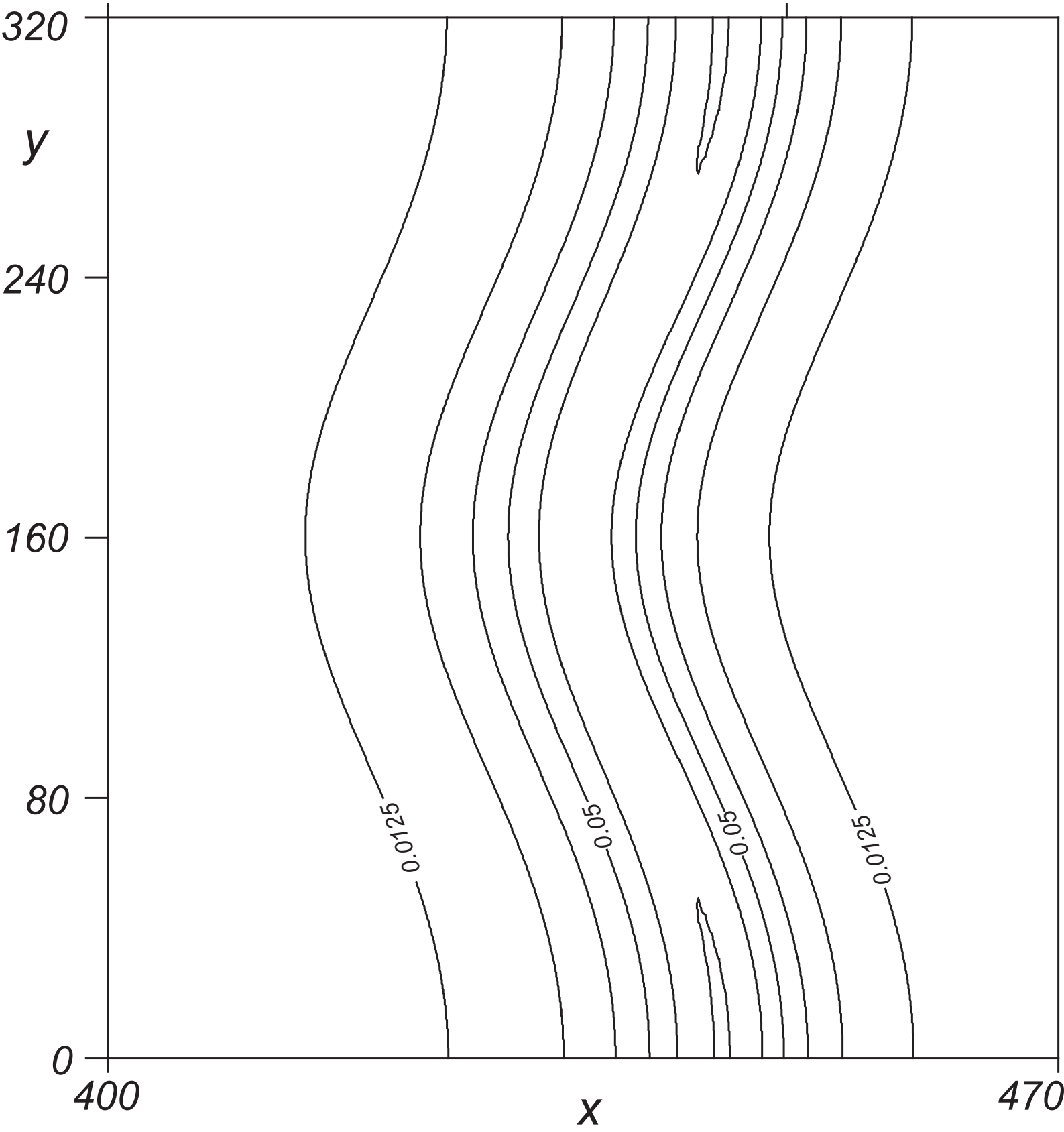

Figure 10

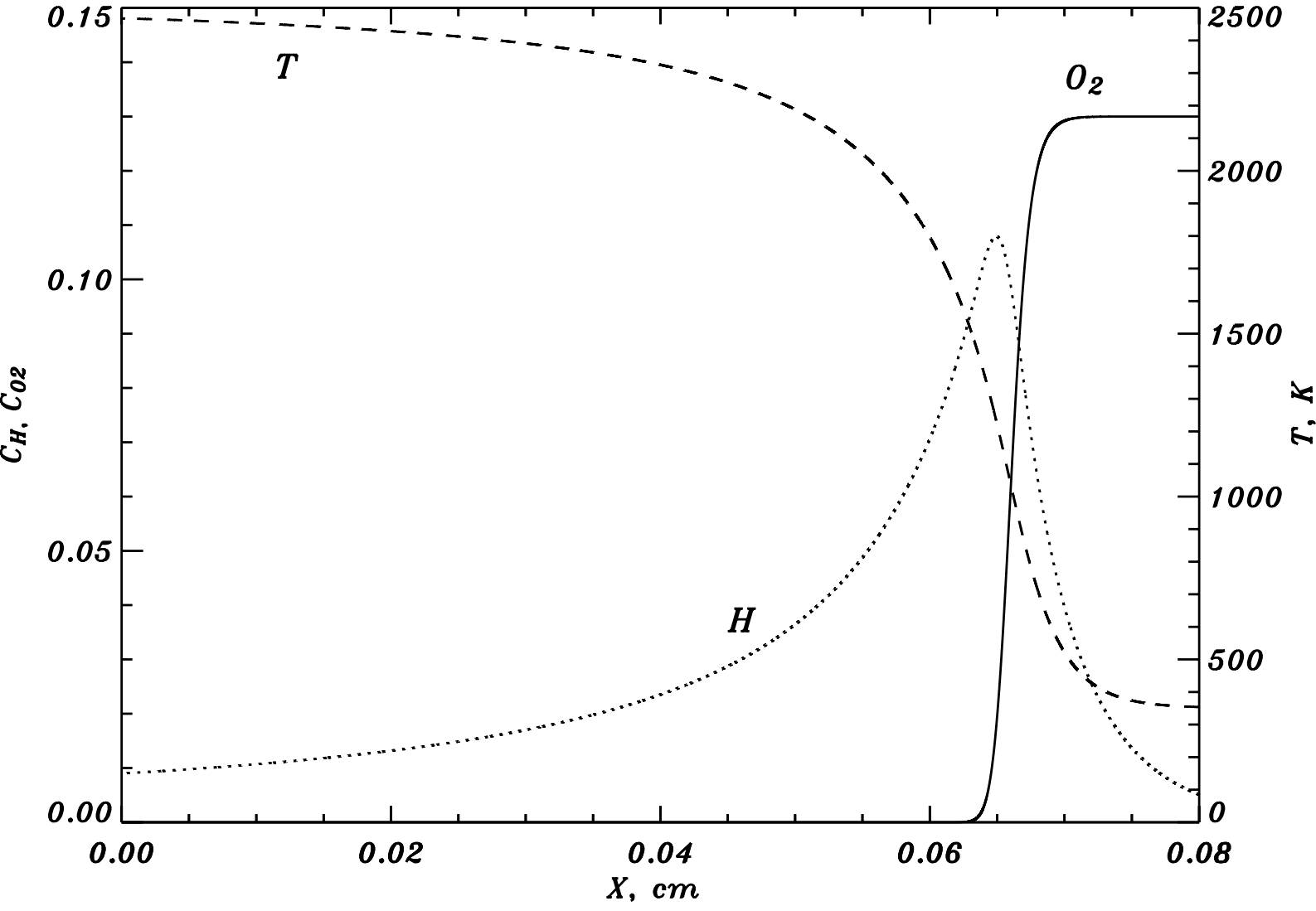
0.15
0.10
0.05
0.00
2500
2000
1500
1000
500
0
T
O2
H
0.00
0.02
0.04
0.06
0.08
X, cm
CH, CO2
T, K